Quantum Electronics **39** (3) 205 – 228 (2009)

REVIEW

PACS numbers: 42.65.Jx; 52.50.Jm; 42.68.Ay
DOI: 10.1070/QE2009v039n03ABEH013916

Filamentation of high-power femtosecond laser radiation

V.P. Kandidov, S.A. Shlenov, O.G. Kosareva

Contents

V.P. Kandidov, S.A. Shlenov, O.G. Kosareva Department of Physics, International Laser Center, M.V. Lomonosov Moscow State University, Vorob'evy gory, 119991 Moscow, Russia; e-mail: kandidov@phys.msu.ru

Received 4 June 2008; revision received 5 December 2008
Kvantovaya Elektronika **39** (3) 205 – 228 (2009)
Translated by M.N. Sapozhnikov

Abstract. **The state of the art of investigations on filamentation of a high-power femtosecond laser radiation in transparent media is reviewed. The physical picture of this phenomenon is presented and its relation to the fundamental concepts of nonlinear optics and practical applications is demonstrated. Experimental and theoretical methods are briefly considered and laser radiation parameters in the case of filamentation are given. The review can be of interest both**

for specialists and researches wanting to become familiar with a new, rapidly developing direction in laser physics.

Keywords*: filamentation, femtosecond laser pulses, self-focusing, plasma channels, supercontinuum, conic radiation, atmospheric optics, microoptics.*

1. Introduction

The phenomenon of laser radiation filamentation, which has been known beginning from the 1960s – 1970s, attracted attention again in the mid-1990s, when extended thin high-energy-density 'filaments' were obtained during the propagation of high-power femtosecond laser pulses in air. The spatiotemporal energy localisation upon filamentation of such pulses in gases and transparent dielectrics is accompanied by the generation of plasma channels, conic emission, supercontinuum radiation, and the enhancement of the nonlinear optical interaction of laser radiation with a medium. The unique properties of filamentation open up new possibilities for using femtosecond laser technologies in atmospheric optics, microoptics, and other applications. The fundamental and applied aspects of this phenomenon have been considered in many papers, including reviews. Investigations performed by the late 1990s were briefly reviewed in paper [1]. Recently, comprehensive reviews [2 – 5] were published. A special issue of Applied Physics [6] is devoted to investigations of a supercontinuum; book [7] published by Springer contains papers presented by leading research groups studying filamentation. Our review presents the state of the art of investigations and physical picture of filamentation of femtosecond laser radiation. The relation between these investigations and studies of the self-focusing and nonlinear-optical interaction of laser radiation with various media performed in the 1960s – 1980s is demonstrated. Applications of filamentation in modern laser technologies are considered.

A luminous filament was observed for the first time in 1965 upon focusing 20-MW nanosecond laser pulses into a cell with organic liquids [8]. It was assumed in earlier papers that a waveguide regime exists during the propagation of an electromagnetic beam [9] and self-focusing appears in the beams when their powers exceeds a threshold value called the critical power [10]. The damage of an optical glass produced by focused laser beams was reported in [11]. The filament parameters and critical power of laser radiation self-focusing in carbon disulfide were determined in [12] by measuring a change in the beam profile with distance. The self-focusing of radiation in air was first observed in [13] for a converging beam and in [14] for a collimated beam. In high-power-density radiation, small-scale self-focusing develops during which a laser beam splits due to the modulation instability of the intense light field in a medium with the Kerr nonlinearity [15]. The damage of optical elements during small-scale self-focusing was observed in experiments with neodymium glass amplifiers [16, 17].

With the advent of high-power femtosecond lasers the generation of extended filaments became possible during the propagation of collimated radiation in gases, in particular, in air at the atmospheric pressure. In the first laboratory experiments with 5 – 50-GW, 150 – 239-fs pulses at 800 nm [18 – 20] in air, the generation of filaments of length up to a hundred meters was observed, which exceeds their Rayleigh length by many times. The colour rings of supercontinuum conic emission were formed around a filament. In the case of 60-fs, 300-GW pulses, the filament length exceeded 200 m [21]. In experiment [22], white light was observed for the first time during scattering of supercontinuum radiation in the atmosphere at altitudes up to 2 km. On the Teramobile Franco-German setup (793 nm, 70 fs, 350 mJ, 6 TW, the beam diameter 5 cm) [23], the 'trace' of fundamental radiation was obtained at altitudes up to 20 km and multiple scattering of the UV wing of a supercontinuum in a haze was recorded at an altitude of a few kilometres [24]. The supercontinuum spectrum measured on this setup covered the range from 300 nm to 4.5 μm [25]. On the Alise setup (1054 nm, 520 fs, 26 J, 32 TW), the formation of a hundred of filaments in a pulse was detected, which generated white light (supercontinuum) propagating up to the altitude exceeding 20 km [26].

The possibility of probing the atmosphere by supercontinuum radiation was demonstrated for the first time in [22, 24]. A femtosecond white light lidar, in which directed broadband pulsed radiation is emitted by a filament generating a supercontinuum, combines the advantages of time-resolved probing and differential absorption spectroscopy. In the first filamentation-induced fluorescence spectroscopy experiments, the remote probing of ethanol molecules [27] and bioaerosols containing riboflavin [28] was performed in air. In remote emission spectroscopy experiments, in which a filament generated plasma at a remote target (laser-induced breakdown spectroscopy), the atomic spectra of copper and steel were recorded [29]. The control of a high-voltage electric discharge with the help of the plasma channel produced by a filament was demonstrated for the first time in [30]. The authors of [31] proposed to use near-IR femtosecond radiation for recording elements of microoptics in glasses.

2. Phenomenon of laser pulse filamentation

2.1 Detection of a filament and its parameters in air

Filamentation during the propagation of femtosecond laser pulses in air is commonly obtained and detected by using a commercial terawatt Ti : sapphire laser with a pulse repetition rate of 10 Hz [32]. Visually, a filament produced by the 800-nm radiation is a long thread luminous due to fluorescence of nitrogen molecules in the intense light field (Fig. 1) [2]. To detect directly the parameters of filaments, a scheme was proposed [33] in which the nonlinear interaction of high-power radiation with the measuring equipment was minimised by using a helium chamber with a gas valve. Due to a low cubic nonlinearity coefficient and a high ionisation potential of a helium atom, the radiation intensity is reduced down to a safe level by retaining the similarity of parameters in the process of linear diffraction of radiation in the chamber.

The method of time-resolved polarisation measurements [34] can be used to detect the instant intensity distribution in a pulse and a change in this distribution along a filament. In this method, a change in the polarisation of a probe beam is measured, which is caused by the nonlinear increment in the refractive index of a medium produced by a high-power pulse forming the filament. In [35], a train of four probe pulses was used, which were separated by time intervals and intersected a filament in several planes along the filament length (Fig. 2). The time-resolved measurements of the

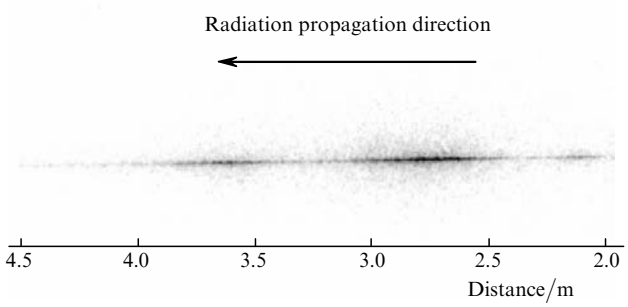

Figure 1. Side view of a filament during the propagation of 800-nm, 13-mJ, 45-fs pulses in air focused by a lens with the focal distance $F = 5$ m. The filament diameter is 100 μm [2].

three-dimensional intensity distribution based on the cross-correlation scheme of sum-frequency generation during the nonlinear-optical interaction of a filament in a crystal with the quadratic nonlinearity were performed in [36, 37]. This technique was modified to the method of gating in spectral measurements allowing to record the evolution of the frequency-angular spectrum during a pulse [38].

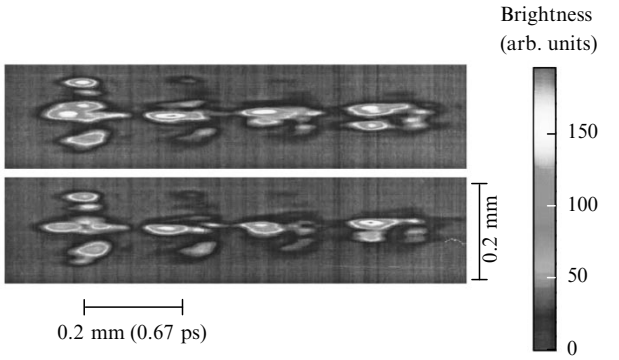

Figure 2. Two side views of a pulse, each of them being obtained for one pulse by the method of time-resolved polarigraphy successively with a displacement of 0.2 mm along a filament in air. The pulse energy and duration are 9.5 mJ and 160 fs, respectively, the geometrical focusing distance is 200 mm. The pulse propagates from left to right. The image brightness is proportional to the product of the square of the filament intensity and intensities of probe pulses shifted in time by 0.67 ps [35].

The parameters of a plasma channel produced upon the multiphoton ionisation of oxygen and nitrogen molecules in a strong field in air can be measured by using various schemes. In [39], the electron density was measured by a change in the resistance of the air gap between the plates of high-voltage electrodes, where the plasma channel of a filament was formed. The interference scheme with a probe beam propagating along the channel [21] was used to estimate the average electron density, while the scheme with a beam perpendicular to the filament [40] was used to measure the lifetime of the laser plasma in air. The possibilities of a shadow scheme with a probe beam perpendicular to the channel for measuring the parameters of the laser plasma were experimentally compared with the interference scheme in [41]. The transverse dimensions of a plasma channel were determined by the method of diffraction of second-harmonic radiation from a Ti : sapphire laser [42, 43]. The electron density distribution along the channel length was measured by the acoustooptic method with a microphone with a narrow directivity diagram [44]. In a scheme with an antenna located close to a filament [45], a change in the sign of the total charge along the channel was detected, which indicates the existence of pondermotive forces in the laser plasma. The method of super-high-speed interferometry was used to obtain the spatiotemporal electron density profiles in plasma and detect its postionisation [46].

During the filamentation of radiation, a spatial mode, close to the Townes mode, is selected, which is a stationary solution of the beam self-focusing equation [10, 47]. This effect, which is called the beam 'self-purification' in the foreign literature, was observed in [48, 49] and discussed in detail in [50].

The parameters of filaments at a fixed radiation wavelength weakly depend on the initial parameters of a laser pulse and are determined by the radiation wavelength and optical properties of a medium. The typical diameter of a filament in air for a radiation wavelength of 800 nm is 100 μm [18 – 20], while the peak radiation intensity achieves 4×10^{13} W cm^{-2} [51 – 53]. According to the first publications, 8 % – 10 % of the pulse energy is localised in a thin filament [20]. The direct measurements [33] of parameters of a filament produced by a 800-nm, 50-fs, 20-mJ pulse propagated a distance 10 m in air gave the filament diameter 130 μm (at the 0.5 level), the filament energy 152 J, the peak radiation intensity 1.3×10^{13} W cm^{-2}, the peak radiation power 2.9 GW, and the energy transferred through the unit area 0.6 J cm^{-2}. The free electron density in the induced laser plasma is $10^{14} - 10^{16}$ cm^{-3} [21, 39, 54], the plasma channel diameter is estimated as 20 – 85 μm [42, 54], its specific resistance is estimated as 1 Ω cm, and the characteristic recombination time of the plasma is 1 – 10 ns [39, 40, 55 – 58]. When the second pulse delayed by 10 ns was used, the plasma lifetime increased up to 200 ns [59, 60]. The attenuation coefficient of the pulse energy during filamentation in air estimated from lidar measurements performed in [61] is $(7.7 - 1.2) \times 10^{-3}$ m^{-1}. The length of a filament (and a plasma channel) in pure air is determined by the energy loss for photoionisation (which is small) and achieves a few meters – tens of metres depending on the experimental conditions. A plasma channel of diameter 150 μm and length 5 m with the average electron density of 10^{18} cm^{-3} was obtained upon filamentation of 25-fs, 15-mJ pulses in air [62]. In the case of multiple filamentation produced by phase-modulated terawatt pulses, continuous plasma channels of length ~ 100 m were observed. As the pulse duration was increased due to phase modulation, these channels decomposed into individual plasma bursts, which were observed at distances up to 370 m (Fig. 3) [63].

In focused radiation, a competition between filamentation and optical breakdown can take place, and the filament and plasma channel parameters strongly depend on the geometrical focusing distance [64]. In the case of weak focusing, filamentation dominates and an extended plasma channel with a low electron density is formed. When the geometrical focusing distance was decreased, both the plasma channel of the filament formed in front of the geometrical focus and the dense optical breakdown plasma in its vicinity were observed. In the case of tight focusing, the filament length becomes too small to be measured, and only the breakdown plasma with the high electron density exists in the geometrical focus of a lens. In experiments with

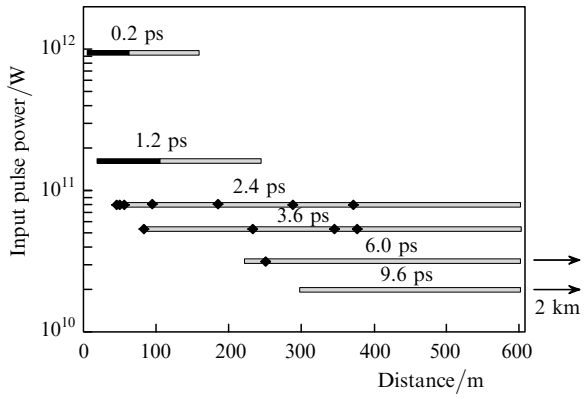

Figure 3. Position and length of filaments as functions of the initial chirp of a laser pulse. A transform -limited pulse has the duration of 100 fs. The dark lines and dots indicate distances at which bright light filaments and plasma were observed in air; the grey lines indicate distances at which only light filaments were observed [63].

807-nm, 45-fs, 60-GW pulses [54], the electron density in air increased from 10^{15} to 2×10^{18} cm^{-3} when the focal distance of a lens was decreased from 380 to 10 cm.

Filamentation in air has been studied mainly at a wavelength of 800 nm emitted by widespread femtosecond lasers with a Ti : sapphire output amplifier. However, one of the key experiments on filamentation on a long path has been performed by using a Nd : YLF laser emitting at 1053 nm [21]. The number of experiments on the filamentation of visible and UV radiation in air is small. In these experiments, the second harmonic of a neodymium glass laser [65] and the second [49, 66] and third [67 – 69] harmonics of a Ti : sapphire laser were used. Filamentation of the parametrically generated 1.54-μm, 100-GW radiation in air and fused silica was studied in [70]. The parameters of filaments and plasma channels in air are presented in Table 1.

2.2 Filamentation in condensed media

The phenomenon of filamentation of near-IR femtosecond laser radiation in condensed media attracts attention first of all because the filament plasma can be used to modify optical materials to fabricate elements of microoptics. The image of a femtosecond filament in fused silica and the change in the refractive index produced by the filament was recorded at a long exposure time in [71] by focusing 130-fs laser pulses with the numerical aperture NA = 0.01. The instant image of the 'trace' of pulsed radiation focused into a silica sample was obtained by the method of time-resolved femtosecond optical polarigraphy [72].

An extended filament can be obtained by weakly focusing radiation on the front face of a sample without its damage. However, in the case of tight focusing of femtosecond radiation on a transparent dielectric, the effect of the interaction of radiation with the sample can be qualitatively different. Focused radiation with energy 2 μJ produces the breakdown plasma with the electron density up to 10^{20} cm^{-3} in a beam waist of diameter 1 μm, resulting in the formation of a diffusion damage region [73]. Behind this region, an extended trace (material modification) produced by the plasma filament channel with the low electron density was observed. Experimental studies [74] showed that only weakly focused radiation could produce the low-density filament plasma, which causes the modification of the refractive index required for recording high-quality waveguides in glass. The possibility of producing an extended plasma channel in fused silica upon axicon focusing of femtosecond radiation was demonstrated in [75]. The filamentation of radiation in a two-component condensed medium was studied in [76].

The image of the plasma filament channel in fused silica was obtained in [77] by scattering the probe radiation from a He – Ne laser (616 nm, 200 fs, 10 μJ). The formation of a channel with the modified refractive index in glass and the relation between this process with the electron density of the laser plasma with increasing the number of 248-nm, 450-fs laser pulses were studied in [78]. The change in the refractive index occurs at the electron density 4×10^{19} cm^{-3} and amounts to 0.4×10^{-3} after irradiation by one pulse, to 1.2×10^{-3} after 100 pulses, and saturates at the 3.5×10^{-3} level after irradiation by 1000 pulses.

The spatiotemporal picture of a change in the refractive index upon filamentation of femtosecond radiation in water was obtained by the shadow method in [79]. The change in the refractive index at the leading edge of the filament caused by the Kerr nonlinearity is positive and is 3×10^{-4}, while at the tail in the plasma channel it is negative and is $(1.2 \pm 0.2) \times 10^{-4}$ (Fig. 4). The longitudinal modulation of variations Δn in the refractive index in the plasma channel at the scale ~ 20 μm is explained by the refocusing of radiation upon filamentation. The formation of an extended filament during the propagation of a pulse in liquid can be also visualised by two-photon fluorescence detected through a side window of a cell [80].

The competition of the optical breakdown and filamentation of focused femtosecond radiation in water, as an example of a condensed medium, was investigated in [81]. As the radiation geometrical focusing distance is increased, the optical breakdown threshold slightly increases, while the supercontinuum generation threshold, characterising filamen-tation, decreases by several times. The energy density distribution in a pulse and the electron density distribution in the laser plasma during breakdown have the shape of a short cone with the dense plasma region at the top and a narrow filament formed behind this region. In the case of weak focusing, a radiation pulse of the same energy produces an extended filament of diameter 5 – 10 μm and a

Table 1. Main parameters of a filament in air obtained in experiments with radiation pulses at different wavelengths.

Wavelength/nm	Filament radius/μm	Radiation intensity in a filament/W cm^{-2}	Plasma channel radius/μm	Electron concentration/cm^{-3}	References
248	100 – 150	10^{12}	–	$3 \times 10^{15} - 10^{16}$	[67 – 69]
406	100	–	–	–	[49]
527	120	6×10^{12}	–	–	[65]
800	80 – 150	$5 \times 10^{13} - 10^{14}$	50 – 65	$10^{16} - 10^{17}$	[18, 19, 40, 42]
1053	100 – 1000	5×10^{12}	–	10^{16}	[21]

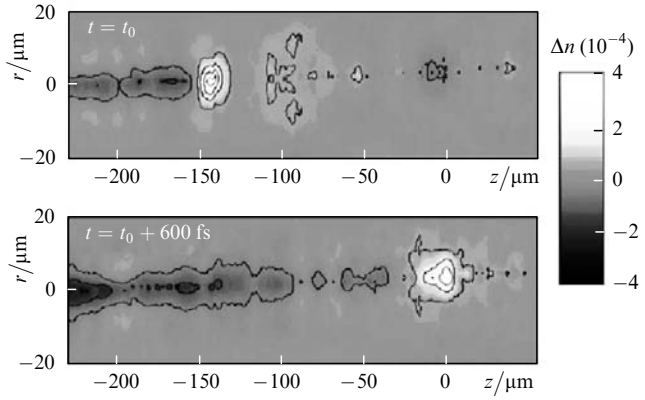

Figure 4. Side views of the change in the refractive index in water upon filamentation of 120-fs pulses. The two images shifted in time by 600 fs are obtained by the shadow method with a transverse spatial resolution of 1.5 μm and a longitudinal resolution of 5.2 μm (23 fs) [79].

plasma channel of diameter 2–5 μm, in which the electron density is considerably lower than that during the breakdown. Filamentation experiments with 527-nm, 200-fs pulses focused into a water cell were performed in [82, 83]. The amplification of radiation in a filament was obtained in the sulforhodamine 640 dye solution in methanol pumped by the 532-nm radiation [84].

2.3 Physical models of filamentation

Filamentation appears due to nonlinear-optical interaction of high-power short laser pulses with a transparent medium. Nonlinear optical effects caused by the absorption of laser energy (thermal self-action, refraction by acoustic waves, etc.) are too slow for femtosecond radiation and the interaction of this radiation with a medium is determined by the Kerr nonlinearity and nonlinearity of the laser plasma produced upon photoionisation in a strong light field of the filament. The nonlinear increment Δn_{K} of the refractive index n_0 caused by the Kerr nonlinearity is positive and proportional to the field intensity I:

$$\Delta n_{\mathrm{K}} = n_2 I, \tag{1}$$

where n_2 is the coefficient of the cubic nonlinearity of the medium; $I = cn_0|E|^2/(8\pi)$; E is the light field strength; and c is the speed of light in vacuum. The increment Δn_{p} of the refractive index in the plasma is negative and is described in the simplest case by the expression

$$\Delta n_{\mathrm{p}} = -\frac{\omega_{\mathrm{p}}^2}{2\omega^2}, \tag{2}$$

where $\omega_{\mathrm{p}} = (4\pi e^2 N_{\mathrm{e}}/m_{\mathrm{e}})^{1/2}$ is the plasma frequency; e, m_{e}, and N_{e} are the electron charge, mass, and concentration, respectively; and ω is the light field frequency. Electrons in gases are first generated due to multiphoton ionisation [85, 86] with the probability proportional to I^K, where K is the ionisation order equal to the number of photons required to ionise the medium. As the radiation intensity is increased, the probability of tunnelling ionisation of atoms and molecules increases. The generation of laser plasma in condensed media occurs due to the transition of electrons to the conduction band under the action of laser radiation and avalanche ionisation at which the electron density in the plasma increases exponentially in time. In the general case, the time dependence of the electron density $N_{\mathrm{e}}(r, z, t)$ upon photoionisation is described by the equation

$$\frac{\partial N_{\mathrm{e}}}{\partial t} = R(I)(N_0 - N_{\mathrm{e}}) + v_{\mathrm{i}} N_{\mathrm{e}} - \beta N_{\mathrm{e}}^2, \tag{3}$$

where N_0 and $R(I)$ are the density and ionisation rate of neutral particles, respectively; β is the coefficient of radiative recombination of electrons and v_i is the avalanche ionisation rate. The contribution of avalanche ionisation to the generation of electrons in gases at the atmospheric pressure is negligible, and the electron density N_{e} during multiphoton ionisation increases according to the power law with time. Because of the exponential and power (with $K \gg 1$) dependences of the ionisation rate on the radiation intensity, the change in the electron density and the appearance of plasma defocusing with increasing the radiation intensity have a threshold. For a wavelength of 0.8 μm, the photoionisation threshold in air is $I_{\mathrm{i}} = 10^{13} - 10^{14}$ W cm^{-2} [51] and in water $I_{\mathrm{i}} \approx 10^{13}$ W cm^{-2} [81].

The intensity of a pulse with the peak intensity exceeding the critical self-focusing power increases with approaching the nonlinear focus. As the peak intensity achieves the photoionisation threshold, a laser plasma is produced, which causes the defocusing of radiation, thereby restricting the intensity increase in the nonlinear focus. The dynamic balance of the Kerr self-focusing and plasma defocusing leads to the stability of parameters in the extended filament of a femtosecond pulse. The balance of these quantities in the filament does not mean that the waveguide regime appears and the self-channeling of the pulse in the medium takes place. At the same time, the first estimates of the light field intensity and electron density in a filament were obtained in [18] based on the model of the self-channeling of a femtosecond laser pulse, which assumes the equality of the phase incursion caused by the Kerr nonlinearity and the phase incursion produced by diffraction and plasma nonlinearity. The model of the waveguide propagation of a femtosecond laser pulse during filamentation was proposed in [19, 87]. According to this model, an extended filament is a quasi-stable leaking mode of an antiwaveguide in which the pulse-induced refractive index of the core is smaller than that of the cladding, while conic emission observed upon filamentation is the Cerenkov radiation.

In [20, 88], the dynamic model of moving foci was developed to interpret the filamentation of femtosecond laser radiation. The moving foci model was proposed for the first time in [89] to explain the quasi-stationary self-focusing of nanosecond laser radiation and was then developed in [90]. This model was experimentally confirmed in papers [90–92]. According to the dynamic moving foci model, a filament represents a continuous set of nonlinear foci appearing in the time slices of a pulse, beginning from a slice corresponding to the peak power, and then successively in slices at the leading edge of the pulse. The time slices of the pulse in the dynamic model are not independent, and intensity redistribution in a slice is determined by processes in previous slices, in which the radiation intensity achieved the photoionisation and laser plasma formation threshold.

The relation between the Kerr and plasma nonlinearities is different in different time slices: at the leading edge the Kerr nonlinearity dominates, while at the trailing edge the plasma nonlinearity dominates, which causes the defocusing of time slices following after focused slices. As a result, the Kerr self-focusing at the leading edge of the pulse is changed to the nonstationary plasma defocusing at the trailing edge due to the increase in the electron density with time upon photoionisation of the medium. Because of this upon filamentation, unlike quasi-stationary self-focusing [89], aberration distortions in the intensity distribution appear in pulse slices after self-focusing. Slices at the trailing edge decompose under the action of the laser plasma into a set of concentric rings in the cross section plane. The nonlinear focus moves to the leading edge of the pulse during its propagation, and the circular structure in the beam cross section covers the increasing part of the time profile of the pulse (Fig. 5) [7, 88, 93]. Circular structures were detected in [94] by the damage of the glass surface on which radiation experiencing filamentation in air was incident. A simple model explaining the formation of rings surrounding filaments in the beam cross section was proposed in [95]. According to this model, rings in the intensity distribution are caused by the interference of a wave at the fundamental frequency, which diverges from the beam axis due to plasma defocusing, with a wave at the beam periphery, which experienced slight distortions and whose wavefront can be assumed plane.

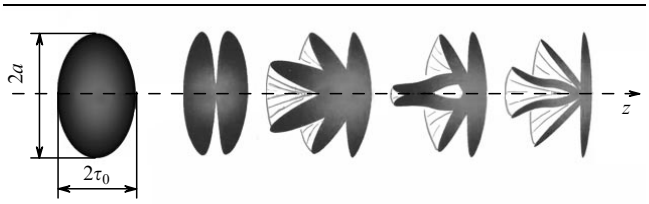

Figure 5. Radiation refocusing during filamentation. The qualitative picture of the change in the intensity distribution in a plane parallel to the pulse propagation direction; τ_0 is the pulse duration.

2.4 Energy reservoir of an extended filament and refocusing

An extended narrow filament with a high light field concentration is formed due to a surrounding energy reservoir which provides the existence of the filament [96]. During the filamentation of radiation, a continuous energy exchange occurs between the axial region of the beam with the high radiation intensity and its periphery with the low intensity [97]. During the formation of the nonlinear focus, the radiation power from the beam periphery 'contracts' to the beam axis, while during defocusing in the plasma, the radiation power from the axial region 'flows' back to the periphery.

The role of the energy reservoir in the formation of an extended filament is clearly confirmed by laboratory experiments. The centre of a filament in [98] was completely blocked by an opaque disc of diameter 55 μm, and only the beam periphery, containing ~ 20 % of the pulse energy, was unblocked. Nevertheless, the filament was interrupted only at a small distance behind the disc and then was recovered over the entire length, as in the absence of the screen. A similar experiment in air, in which a filament was blocked by a suspended drop of diameter 95 μm, was performed in [99]. The key role of the energy reservoir at the beam periphery in the formation of an extended filament is confirmed by a direct experiment [100] in which a thin aluminium foil screen was placed into the beam in air. The intense field of the filament burned a hole in the foil. It was found that a screen with a hole produced by the filament completely blocked filamentation behind it for next pulses because it blocked the beam periphery representing the energy reservoir required for the existence of an extended filament.

When the radiation pulse power exceeds the critical self-focusing power by a factor of 6 – 10, refocusing appears. In this case, the radiation defocused in the plasma in time slices at the trailing edge of the pulse again 'contracts' to the beam axis due to the Kerr self-focusing, thereby increasing the energy density at the beam axis (Fig. 5). The refocusing effect, observed for the first time in [20], was theoretically studied in [1, 88]. By measuring fluorescence of nitrogen molecules in air, the authors of [101] observed refocusing in a converging beam, which leads to the formation of the second intensity maximum behind the geometrical focus of a lens [2]. The refocusing of time slices in the dynamic moving foci model explains the observation of a filament in focused radiation behind the geometrical focus of a lens [87].

The influence of the air pressure on refocusing during filamentation of focused radiation was considered in [52]. In a medium with a strong material dispersion, multiple refocusing can occur at which a continuous filament degenerates to a sequence of 'hot' dots with high energy density [102].

2.5 Filament generation

The dynamic moving foci model allows one to determine a distance to the filamentation onset based on simple considerations. At the initial stage of filamentation, a nonlinear focus is formed, the radiation intensity does not exceed the photoionisation threshold of a medium, and the light field changes only due to the Kerr self-focusing. For pulses of duration of a few tens or hundreds of femtoseconds, filamentation in air and, as a rule, in optical glasses begins at distances that are considerably smaller than the dispersion length, and the influence of the material dispersion on the generation of filaments can be neglected. By neglecting the delay of the nonlinear response of a Kerr medium irradiated by a femtosecond pulse, the distance to the filament formation can be estimated by using the stationary self-focusing model. In this model, the time slice of a pulse corresponding to the peak power is focused at the smallest distance, thereby determining the filamentation onset. The distance $z_{\rm fil}$ to the filament beginning coincides with the self-focusing length of a cw radiation beam with power equal to the peak pulse power P_0. The stationary self-focusing length was described in [103] by the empirical formula

$$z_{\rm fil} = \frac{0.367ka^2}{\{[(P_0/P_{\rm cr})^{1/2} - 0.852]^2 - 0.0219\}^{1/2}}, \qquad (4)$$

obtained by generalising the results of numerical investigations. Here, a is the beam radius at the e^{-1} intensity level; $k = 2\pi/\lambda$ is the wave number; $P_{\rm cr} = R_{\rm cr}\lambda^2/(8\pi n_0 n_2)$ is the critical self-focusing power; $R_{\rm cr}$ is the nonlinearity

parameter ($R_{cr} = 3.77$ for an axially symmetric collimated Gaussian beam).

The critical power depends on the radiation intensity distribution in the beam. For a beam with profile coinciding with the Townes mode [10], the power P_{cr} is minimal, and the corresponding nonlinearity parameter is $R_{cr}^{T} = 3.72$ [104]. For beams with the intensity distribution without the axial symmetry, the critical self-focusing power increases due to the 'leakage' of their power during the formation of the axially symmetric Townes mode. Thus, it was found that the critical power $P_{cr}(a/b)$ for beams with the elliptic intensity profile increases by several times with increasing the axial ratio a/b of the intensity distribution [105, 106].

The influence of the polarisation of a light field on the filamentation of radiation was studied in [107], where its was shown that the distance z_{fil} to the filament onset in the case of linear polarisation was smaller than that in the case of circular polarisation due to a higher nonlinearity coefficient n_2 and, hence, a lower critical power P_{cr}.

According to experimental data obtained by different methods, the cubic nonlinearity coefficient n_2 of air for nanosecond radiation at a wavelength of 800 nm was estimated as $(1.92 - 5.57) \times 10^{-19}$ cm^2 W^{-1} [108 – 110]. Correspondingly, the critical self-focusing power in air is 5 – 1.72 GW. The dependences of the cubic susceptibility of nitrogen and oxygen on the radiation wavelength were determined in [111] from experimental data. The wavelength dependences of the nonlinearity coefficient n_2 and critical power P_{cr} in air at the atmospheric pressure, obtained based on the known experimental data, are presented in [112].

The cubic nonlinearity coefficient for femtosecond radiation at 800 nm in water is 4.4×10^{-16} cm^2 W^{-1} [113] and the critical self-focusing power is 4.2 MW [114]. According to the measurements performed with picosecond pulses [115], the critical self-focusing power in water at 1.06 μm is 2.34 MW. This power for fused silica is 2.3 MW [116].

The nonlinear increment Δn_K of the refractive index in optical glass is mainly caused by the electronic component, and the delay time of the nonlinear response does not exceed 10 fs [117]. Therefore, the cubic nonlinearity of glass irradiated by pulses of duration of a few tens of femtoseconds can be considered inertialless. The increment Δn_K in gases is determined by the electronic nonlinearity and stimulated scattering by the rotational transitions in molecules, which causes the delay of the electronic response with the characteristic time $\tau_{nl} \approx 70$ fs in air [109, 118, 119]. In [96, 120], the approximation was proposed to describe the time dependence of the increment Δn_K in air. To estimate the distance to the filamentation onset by expression (4), the effective nonlinearity coefficient $n_2^{eff}(t)$ was introduced in [95, 121] for a time slice in a pulse with the specified intensity profile $I(t)$ and the quasi-stationary estimate of the critical self-focusing power was obtained.

3. Pulse spectrum transformation

The generation of a supercontinuum and conic emission by femtosecond radiation occurs due to a strong nonlinear-optical interaction of an electric field with a medium, which is achieved owing to the high spatiotemporal localisation of the light field. Conditions for the generation of a supercontinuum can be obtained in optical guiding systems such as capillaries [122], optical fibres [123], and photonic crystals [124]. Due to the mode dispersion of radiation in guiding systems, it is possible to obtain the high light field intensity at a comparatively large length, which provides the high efficiency of the nonlinear-optical conversion of the frequency spectrum of the pulse.

In a transparent medium, gas, liquid, optical glass, the localisation of the light field is achieved due to nonlinear-optical effects of beam self-focusing and pulse a compression, and also due to the geometrical focusing of radiation. A filament in a transparent medium is a self-focusing guiding system, in which spatial filtration occurs and the fundamental mode is separated on the axis. A considerable length of a filament, the high energy concentration, the stability of parameters along the entire filament length, and the interaction time of radiation with the medium (a few tens femtoseconds) produce unique conditions for nonlinear-optical interaction, which can be called the nonlinear optics of filaments [50]. This optics includes supercontinuum generation during the propagation of a femtosecond pulse in a transparent dielectric. The efficiency of conversion of laser radiation to a white light pulse upon filamentation is lower than in the case of optical fibres or photonic crystals. However, filamentation does not require special devices and allows one to form a white light source in a specified region of a transparent medium.

3.1 Supercontinuum generation

In one of the first experiments on supercontinuum generation, 0.1-μJ picosecond pulses were focused to a CS_2 cell [125]. The formation of filaments in focused radiation was accompanied by the broadening of its spectrum, which was explained by the self-phase modulation in the medium with cubic nonlinearity. According to theoretical study [126], the spectrum becomes asymmetric, being broadened predominantly to the Stokes region due to the delay of the nonlinear response of the medium. The formation of asymmetric supercontinuum spectra upon focusing the second harmonic of a picosecond neodymium laser to optical crystals and glasses [127] was explained in [128] by the self-phase modulation of radiation caused by the electronic component of the Kerr nonlinearity.

During the filamentation of laser pulses in gases, the spectrum broadens due to the self-phase modulation of radiation and is determined both by the Kerr and plasma nonlinearities whose responses are substantially nonstationary in the femtosecond range. Filamentation accompanied by the generation of a supercontinuum in the range from 150 to 900 nm was observed in [129] upon weak focusing of 790-nm, 125-fs, 2-TW laser pulses to a tube of length 9 m filled with noble gases at the atmospheric pressure. In a scheme with two cells in tandem filled with argon at the atmospheric pressure [130], 805-nm, 45-fs, 1-mJ pulses, whose duration decreased down to 11 fs after filamentation in the first cell, were weakly focused to the second cell to obtain the supercontinuum spectrum covering the range from 250 to 1000 nm in the case of optimal pulse parameters. By using a prism compressor, 70-fs, 0.7-μJ pulses in the range 270 – 290 nm were obtained from the short-wavelength wing of the supercontinuum.

In experiments with terawatt pulses from Ti : sapphire lasers in open atmosphere, a supercontinuum generated in a filament of length more than 20 m was recorded [25]. Upon irradiation by 100-fs pulses, the supercontinuum covered the range from 0.5 to 1.6 μm, while in the case of 35-fs pulses,

the supercontinuum broadened to the IR region up to 4.5 μm (Fig. 6). In the case of pulses with the negative initial phase modulation, at which their duration increased up to 55 fs, the efficiency of radiation conversion to the IR region of the supercontinuum increased. The cross-correlation maps of intensity fluctuations of the spectral components of the supercontinuum obtained upon filamentation of radiation at 815 nm in air show that the self-phase modulation dominates in the supercontinuum generation [131]. The influence of radiation polarisation on the supercontinuum generation in air was experimentally studied in [132] for focused 800-nm, 25-fs, 650-mJ pulses. The higher efficiency of conversion to the short-wavelength region in the case of circular polarisation compared to linear polarisation is explained by a decrease in the Kerr nonlinearity coefficient leading to the increase in the filament length and, therefore, in the nonlinear-optical transformation length. It was shown numerically in [133] that the supercontinuum width at the 10^{-5} level normalised to the central wavelength λ was 0.5 for $\lambda = 248$ nm, 1.0 for $\lambda = 800$ nm, and 1.5 for $\lambda = 1550$ nm.

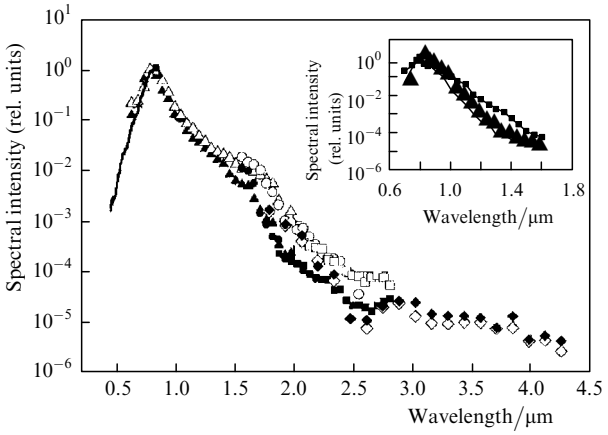

Figure 6. Supercontinuum spectrum measured during filamentation of the 800-nm, 2-TW pulses in air: a 35-fs transform-limited pulse (dark dots); a pulse with the negative initial phase modulation stretched up to 55 fs (light dots). The inset shows the spectra of 100-fs pulses with energies 200 and 100 mJ and peak powers 2 (■) and 1 TW (▲), respectively [25].

According to calculations, the efficiency of laser pulse energy conversion in air to the blue region of a supercontinuum can achieve 5 % – 10 % [134]. In one of the first experiments [135], the supercontinuum energy within the 1 – 1.5-μm band was ~ 7 % of the 800-nm pulse, which is explained by a large length of the nonlinear interaction of radiation in the atmospheric path.

The spectrum of a low-energy pulse (0.4 – 1.8 μJ) in water slightly increases symmetrically due to the self-phase modulation under the conditions of Kerr nonlinearity. In the case of a high-energy pulse (2 – 260 μJ), a filament with a plasma channel is formed, in which the self-phase modulation leads to the blue shift of the spectrum and its broadening by a few hundreds nanometres [53]. The key role of the material dispersion in the broadening of the spectrum during the filamentation of a pulse in a condensed medium was pointed out in theoretical paper [136].

The energy gap width in condensed media strongly affects the broadening of a pulse spectrum during its filamentation. A considerable broadening of the pulse spectrum, which can be treated as supercontinuum generation, is achieved only when the energy gap width W exceeds the laser photon energy $h\nu$ more than by three times [137]. The general conclusion about the width of a supercontinuum generated in condensed media by femtosecond laser pulses is formulated in [138] based on the results of experiments performed with different optical materials irradiated by pulses at 262, 393, and 785 nm. It was found that the generation threshold of the anti-Stokes components of the supercontinuum is determined by the condition $W/(h\nu) \geqslant 2$, and the broadening to the anti-Stokes region increases with increasing the ratio $W/(h\nu)$ (Fig. 7). The spectrum of a 801-nm, 42-fs pulse with the peak power $P_0 = 100P_{cr}$ in barium fluoride symmetrically broadens without shift, while for $P_0 = 3600P_{cr}$ the spectrum shifts to the blue by 20 nm and broadens asymmetrically up to 500 nm [139, 140].

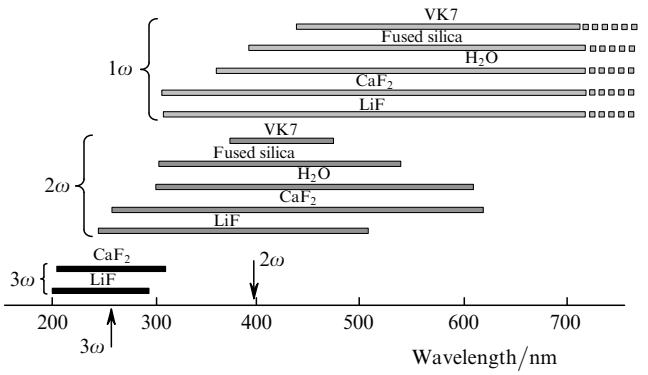

Figure 7. Supercontinuum bands measured in different condensed media during filamentation of focused radiation at wavelengths 785 nm (1ω), 393 nm (2ω), and 262 nm (3ω). The radiation intensity in the focus is $\sim 10^{13}$ W cm^{-2} [138].

3.2 Conic emission and X-waves

The relation between the spectral intensity of the short-wavelength components of the spectrum with their spectral distribution was established for the blue wing of a supercontinuum in [141] for picosecond and femtosecond radiation at 600 nm and in [142] for the third harmonic of femtosecond radiation (80 fs) at 800 nm propagating in inert gases. Experiments on filamentation in water and heavy water with 1.06-μm, 22-ps, 35-mJ laser pulses showed that the divergence of the spectral components of a supercontinuum in the anti-Stokes region is independent of the geometrical focusing distance of radiation and increases with their shift to the blue [143]. This phenomenon, which was called the conic emission of a supercontinuum, was explained by the author of [143] by the Cerenkov radiation on the filament surface. This interpretation is based on the introduction of the phase velocity to a plasma filament channel in the waveguide model of an extended filament, which exceeds, according to (2), the speed of light in the air shell surrounding the channel [19]. The increase in the angular divergence of the supercontinuum with increasing the frequency of spectral components, which was observed upon focusing to an ethylene glycol jet, was explained in [144] by the four-

photon parametric generation of a supercontinuum on the filament surface.

Many papers devoted to the analysis of the mechanism of formation of conic emission point out the relation between the spatial and temporal phase modulations of radiation in a nonlinear medium (see, for example, 145]). According to the concept about the relation between the spatial and temporal parameters of laser radiation in the case of nonlinearity, the angular divergence of spectral components increases with their shift to the blue because a higher phase gradient in time in the expression for the nonlinear increment of the refractive index is related to its higher spatial gradient [146].

The increase in the divergence angle θ with increasing the anti-Stokes shift of spectral components of conic emission upon filamentation of femtosecond laser radiation in air was studied experimentally and numerically in papers [20, 93, 147, 148]. The characteristic angle of deviation θ from the axis for conic emission at 500 nm is $\sim 0.12^\circ$ in the case of filamentation of radiation from a Ti : sapphire laser. The increase in the divergence angle of conic emission at 400 nm with increasing the blue shift was obtained in [49]. According to experiments [149] (527 nm, 200 fs, 3 mJ), the deviation angle θ during filamentation in air linearly depends on the frequency shift $\Delta\omega$ of its spectral components.

The enrichment of the frequency-angular emission spectrum caused by nonlinear-optical interaction of the light field is related to the spatiotemporal transformation of the pulse shape. Filamentation is accompanied by the sharpening of the pulse and spatial compression of its time slices at the leading edge. In addition, the aberration defocusing of subsequent slices occurs in the induced laser plasma, the fundamental radiation is produced in the form of diverging rings, which are compressed during refocusing and, finally, the pulse decomposes into subpulses with the sharpened trailing edge due to the wave nonstationarity. (The term 'wave nonstationarity' introduced in book [150] is translated in the Anglophone literature as 'self-steeping'.) The blue wing of a supercontinuum at the filament onset is mainly generated in defocusing rings at the trailing edge of the pulse, by producing conic emission (Fig. 8) [151]. Then, decomposition into subpulses occurs, and due to the increase in their steepness at the trailing edge, the high-frequency components of the spectrum appear, propagating along the axis. The generation of intense anti-Stokes components in a broad spectral band is caused by an 'optical shock' wave, which is formed in the medium during the increase in the steepness of the trailing edge of the pulse due to the self-steeping during the spatiotemporal pulse compression [151, 152]. The duration of this short-wavelength component pulse is determined by the width of its trailing edge. This is confirmed by experiments with 800-nm, 12-fs pulses [153] in which filamentation in argon ceased when the gas pressure was drastically decreased, which provided the suppression of the dispersion spread of a broadband pulse of the supercontinuum. When the short-wavelength radiation was separated from the supercontinuum by a dielectric mirror, a 9.7-fs, 290-nm UV radiation pulse of width 65 nm was formed.

The notion of the broadening of the frequency spectrum of a pulse due to the self-phase modulation of the light field in a nonlinear medium and the concept of the inseparable relation between temporal and spatial variations in the pulse and, hence between its frequency and angular spectra form the basis of the theory of conic emission of a supercontinuum in a filament [2, 93, 147, 151]. The phase incursion $\varphi(\boldsymbol{r}, z, t)$ of the light field during self-modulation in medium with the Kerr (1) and plasma (2) nonlinearities is a spatiotemporal function, which can be written in the form

$$\varphi(\boldsymbol{r}', z, t') = \varphi_0(\boldsymbol{r}', z, t') + \Delta\omega(\boldsymbol{r}', z, t')t' +$$

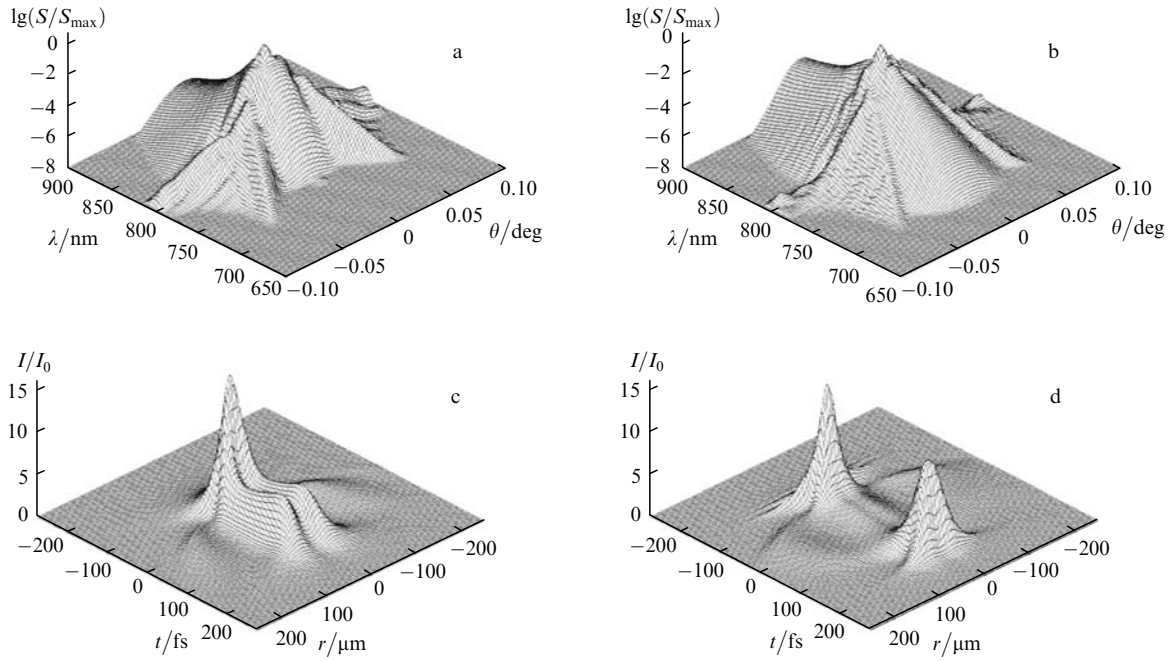

Figure 8. Frequency-angular dependences of the spectral intensity $S(\theta, \lambda)$ (a, b) and spatiotemporal intensity distributions $I(\boldsymbol{r}, t)$ of a pulse at distances $z = 0.43L_d$ (a, c) and $0.6L_d$ (b, d) during filamentation in air. The pulse duration is 150 fs, the beam radius is 3.5 mm, the initial peak intensity is $I_0 = 10^{13}$ W cm^{-2}, the peak power is $6.3P_{cr}$, and the diffraction length is $L_d = 96$ m [151].

$$+\Delta\boldsymbol{k}_{\perp}(\boldsymbol{r}',z,t')\boldsymbol{r}'+\Delta^2\varphi, \quad (5)$$

where $\Delta^2\varphi$ is the term containing the second and higher derivatives of the phase $\varphi(\boldsymbol{r}',z,t')$. The frequency increment $\Delta\omega$ (or wavelength $\Delta\lambda$) of the light field is determined by the time derivative of the induced phase $\Delta\omega=\partial\varphi/\partial t$, while the change in the transverse component of the wave vector $\Delta\boldsymbol{k}_{\perp}$ (or the divergence angle $\theta=\Delta k_{\perp}/k$ of the spectral component) is determined by the spatial gradient of the phase $\Delta k_{\perp}=\operatorname{grad}\varphi$ in the cross section. In [154], the spectral and angular maps of emission in a filament were obtained, which show that the sources of the short-wavelength of the supercontinuum are located at the trailing edge of the pulse whose steepness increases due to self-steeping. In this case, diverging conic emission is mainly formed in the vicinity of edge phase dislocations in ring structures, where both temporal and spatial phase gradients are especially large. The low-frequency spectral components are mainly generated at the leading edge of the pulse. Because of this, the long-wavelength wing of the supercontinuum is recorded in the form of an axially symmetric maximum on the axis, while the short-wavelength wing is observed in the form of concentric rings. When radiation is focused with an axicon, the filament decomposes into an equidistant sequence of conic-emission sources. The interference of emission from these sources leads to the splitting of the continuous angular spectrum of conic emission into narrow rings separated by interference minima [155, 156].

The concept of X-waves used to interpret the filamentation phenomenon is based on the representation of a pulse in the form of a packet of conic waves. The near-field intensity distribution in the $\boldsymbol{r},t$ coordinate space and the far-field intensity distribution in the θ,λ coordinate space upon filamentation in a medium with the normal dispersion have the characteristic X-like shape. X-waves are especially clearly observed in condensed media, for example, in water during the filamentation of radiation with the central wavelength lying in the visible range (Fig. 9) [157]. For 'green' radiation at 527 nm in water, conic waves shifted to the red and blue regions have close intensities, whereas for IR radiation in air at 800 nm, they exist only for the anti-Stokes components of the spectrum. It was shown numerically [158] that, in the case of a competition between diffraction, normal dispersion, and Kerr nonlinearity stationary, weakly localised X-wave can exist, which are the solutions of the nonlinear Schrödinger equation for the pulse envelope. The detection of X-waves in the near- and far-field femtosecond radiation in water [159] and air [160] confirms that the concept of X-waves can be used in investigations of filamentation [157, 161–163].

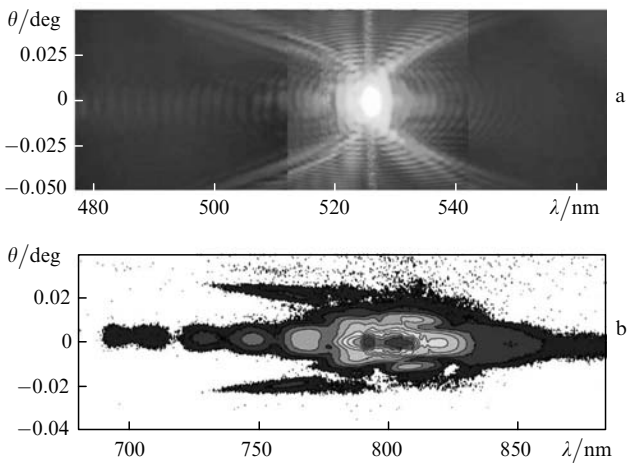

Figure 9. Frequency-angular dependences of the spectral intensity $S(\theta,\lambda)$ of a supercontinuum measured in the far field during the filamentation of the 527-nm radiation in water (a) and the 800-nm radiation in air (b) [157].

The divergence angle of conic emission in a medium with anomalous dispersion decreases with increasing the anti-Stokes shift of spectral components [164, 165], and the pulse spectrum in the θ,λ coordinates has an elliptic shape unlike the X-like shape in the case of normal dispersion [166].

3.3 Frequency conversion and terahertz radiation generation

Third harmonic generation in the optical breakdown plasma in air during focusing of femtosecond laser pulses was observed in [167]. As the incident pulse energy exceeded a threshold, the increase in the third harmonic energy slowed down, which was explained, in the opinion of authors of [167], by spatial and temporal self-action effects. At the same time, these effects produce during filamentation the conditions for the nonlinear-optical conversion of an extended filament in a plasma channel. Third harmonic generation during filamentation of femtosecond radiation at 800 nm was studied in [168]. Due to the nonlinear phase matching of third harmonic and fundamental radiations, the efficient conversion length considerably exceeds the length of their coherent interaction in air. As a result, a 'two-colour' filament is formed. In experiments with 800-nm, 45-fs, 0.5-mJ pulses focused by a lens with the focal distance $F=100$ cm, the length of a 'two-colour' filament was ~ 10 cm, while the third harmonic intensity was 0.1 % of the pump intensity. Due to the clamping of the pump intensity upon filamentation, the third harmonic conversion efficiency is low and weakly depends on pump parameters. The third harmonic conversion efficiency for optimal focusing length and power was 0.12 % for 800-nm, 340-fs, 30-mJ pulses [169] and 0.2 % for 1.54-μm, 300-fs, 30-mJ pulses [70], and 0.13 % for Ti : sapphire laser radiation focused to argon at the optimal pressure 500–700 Torr [170].

Investigations of the spatial distribution of third harmonic radiation showed that phase-matching conditions were fulfilled both on the filament axis and in its ring structure [171]. For the third harmonic beam coaxial with the pump beam, this condition is preserved over the large length of the filament and its intensity increases exponentially with pump power. The diverging third harmonic radiation appears at the filament onset, its intensity first increases and then saturates with increasing pump power. It follows from spatially resolved spectral measurements with 800-nm, 50-fs, 20-mJ pulses [172] that the third harmonic dominates in the supercontinuum generated in the region surrounding the filament. In this case, emission from this region is better reproduced from pulse to pulse than the short-wavelength supercontinuum emission appearing due to self-phase modulation.

The generation of higher harmonics upon filamentation was demonstrated in paper [173]. A filament formed in air

during the propagation of radiation at 800 nm was introduced through a 100-μm-thick quartz window into a cell filled with xenon. The cell length and xenon pressure in it were varied in a broad range. In the cell of length 35 mm at the xenon pressure 38 Torr, the generation of harmonics up to the 15th was obtained. The generation of higher harmonics, from the 45th to 91st, was obtained in [174] upon filamentation of 800-nm, 430-fs, 5-mJ pulses in a cell filled with helium at a pressure of 80 Torr. It was found that these harmonics were generated in the region between two foci during the refocusing of radiation in a filament, where diverging radiation changes to converging.

The frequency conversion of 800-nm, 45-fs pulses upon degenerate four-wave mixing in the case of filamentation in air and argon was performed in [175]. The initial radiation in the 1.1 – 2.4-μm band propagating along the filament axis was converted to a visible radiation pulse of duration up to 12 fs whose wavelength could be tuned from 475 to 600 nm. The conversion efficiency achieved 25 % of the initial pulse energy in the long-wavelength region of the output radiation and decreased down to 5 % – 10 % in the short-wavelength region. Upon four-wave mixing of the 800-nm radiation and its second harmonic in filaments in neon, 12-fs, 26-μJ pulses at 260 nm were obtained, while in the cascade process, 2-μJ, 200-nm pulses were generated [176].

Terahertz radiation emitted in the direction perpendicular to the filament axis was obtained in [177]. The radial radiation intensity at frequencies 94 and 118 GHz remained constant along a plasma channel of length 1 m in air. In xenon, which has a higher nonlinearity coefficient and the relatively low ionisation potential compared to air, the generation of terahertz radiation is more efficient [178]. Terahertz radiation directed forward at a small angle to the filament axis has a higher intensity (Fig. 10) [179]. The angle decreases with increasing the geometrical focusing distance of radiation and, hence, the length of a produced plasma channel [180]. Terahertz radiation has the radial polarisation independently of the laser pulse polarisation. Terahertz radiation directed forward is interpreted as the transfer Cerenkov radiation produced by longitudinal dipole-like charges [45], which are formed behind the ionisation front in the filament and are transferred together with the pulse at the speed of light.

There also exist other models explaining the nature of terahertz radiation of filaments. According to [181], terahertz radiation is produced by the currents of the induced plasma, which appear under the action of pondermotive forces and propagate together with the laser pulse. The characteristic frequency of terahertz radiation is determined by the duration of the pulse envelope and is independent of the plasma frequency. Based on experiments performed in [182] for focused radiation, it was concluded that terahertz radiation is mainly generated due to the degenerate four-wave mixing of the pump and second harmonic radiation appearing in the induced plasma. Under the condition of multiple filamentation, the coherence and polarisation state of terahertz radiation are violated due to the phase shift of radiation of individual plasma channels [180]. When a longitudinal electric field of strength a few kilovolts is applied to a plasma channel, intense depolarised and incoherent terahertz radiation appears, which is interpreted by the authors of [180] as the thermal radiation of air heated due to joule losses in a current-conducting plasma channel.

3.4 Pulse compression

The broadening of the frequency spectrum of a pulse upon generation of a supercontinuum in a filament opens up the possibilities of generating ultrashort pulses directly in the medium. The use of a filament instead of guiding systems provides a considerable increase in the energy of compressed pulses. In [183], weakly focused 800-nm, 42-fs, 0.84-mJ pulses propagated through two extended cells in tandem filled with argon at a pressure of ~ 1 atm, in which the spectrum was broadened due to self-phase modulation upon filamentation. Compressors based on chirped mirrors, which were placed behind each of the cells, compensated the phase modulation of radiation. The pulse duration behind the first cell decreased down to 10.5 fs, its energy being 94 % of the initial energy, and behind the second cell the pulse duration was 5.7 fs, its energy 45 % of the initial

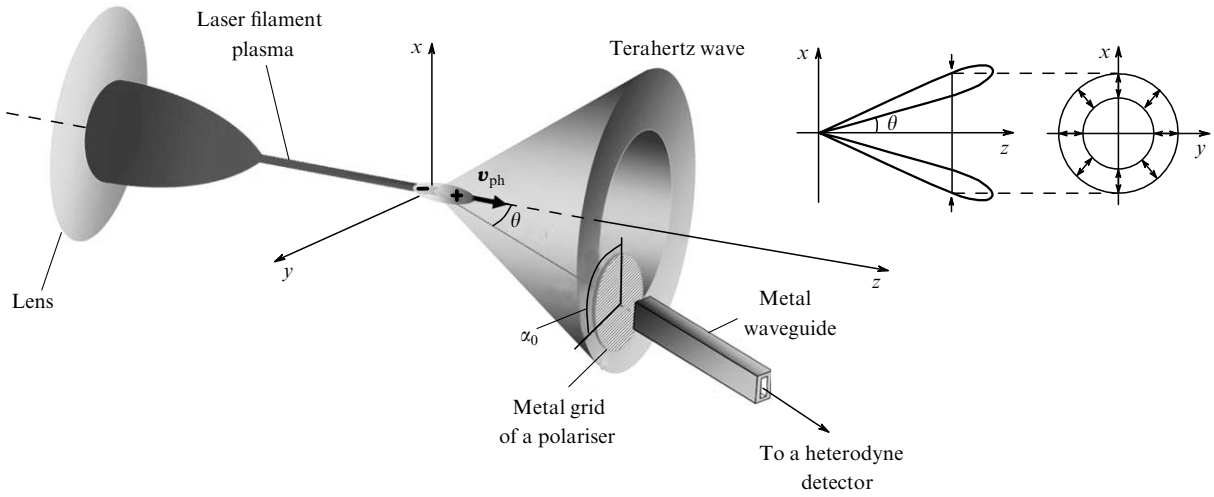

Figure 10. Qualitative experimental scheme for generating terahertz radiation during filamentation of focused radiation in air. The pulse duration, energy, and repetition rate are 150 fs, 4 mJ, and 10 Hz, respectively. The aperture diameter is 5 mm and the focal distance of a lens is 2 m; v_{ph} is the phase velocity. Terahertz radiation was detected with a 91 – 110-GHz heterodyne detector. The inset shows the direction of polarisation in a terahertz radiation cone [179].

energy. When better mirrors were used to compensate for phase modulation, the output pulse duration decreased down to 5.1 fs [184]. The use of higher-power input pulses of energy 2 mJ and the spatial filtration of radiation by 'soft' apertures to suppress multiple filamentation in cells provided the increase in the pulse energy up to 0.7 mJ in a two-stage compression scheme, the pulse duration and repetition rate being 5 fs and 1 kHz, respectively [185].

During filamentation a radiation pulse splits into subpulses after refocusing, and providing conditions for the formation of only one shortest-wavelength pulse, it is possible to compress it without additional compressing devices. Thus, the duration of a 750-nm, 150-fs, 1-mJ pulse decreases down to 30 fs in a cell with methane of length 80 cm with increasing pressure up to 6 – 7 atm, and then the pulse splits into subpulses [186]. Based on the results obtained for various gases and fused silica, the authors of [186] concluded that the self-compression of a high-intensity pulse is a general phenomenon, which can be observed in various dispersive nonlinear-optical media. This conclusion is confirmed in paper [187], where the pulse duration after filamentation in a VK7 glass decreased from 50 to 20 fs. The authors of [188] determined the region of a filament for collimated radiation in air where the maximum compression of a pulsed was achieved. It was shown that the duration of a 805-nm, 55-fs, 4-mJ pulse under these conditions decreased to 9 fs. The possibility of the pulse-duration reduction down to an optical cycle upon filamentation in gas with a pressure gradient for suppressing refocusing was studied numerically in [189].

The pulse compression in the mid-IR range during filamentation was achieved for the first time in [48]. The 2-μm, 55-fs, 0.33-mJ pulses were weakly focused to a 1-m-long cell filled with xenon at a pressure of more than 2 atm to obtain an extended filament. Due to spectral broadening upon filamentation, a highly stable 17-fs, 0.27-mJ pulse corresponding to one spatial mode with the phase-matched carrier was formed at the cell output.

4. Multiple filamentation

Pulsed radiation with the peak power exceeding the critical self-focusing power by more than an order of magnitude produces multiple filaments. This is the inevitable consequence of the spatial-modulation instability of the intense light field in a medium with the cubic nonlinearity [15]. The initial stage of multiple filamentation is determined by the small-scale self-focusing in the time slices of the pulse where nonlinear foci are formed. The centres of creation of nonlinear foci are perturbations of the intensity and phase of the light field, which can be caused by the distribution of radiation at the output aperture of a laser system, by natural fluctuations of the refractive index in the medium and scattering by particles.

4.1 Formation of multiple filaments

The formation of nonlinear foci at the initial stage of creation of multiple filaments causes the intensity redistribution in the beam cross section, which depends on the pulse energy and perturbation geometry at the laser system output. In experiments [21], the formation of three – four maxima of the energy density in the beam cross section was observed at small distances, not all of them producing filaments. In [190], a beam with the non-unimodal energy density distribution in the cross section and the peak power exceeding the critical self-focusing power by 25 times first decomposed, by forming two maxima in the cross section, which then merged to form one filament. As shown in paper [191], the energy competition appears between nonlinear foci formed from closely located perturbations, which can delay the onset of filament formation during the pulse propagation. As a result, the distance to the filament generation does not decrease monotonically with increasing pulse power but increases in the vicinity of powers at which the number of filaments increases. The decomposition of a beam with the azimuthal modulation of the intensity distribution in the cross section was numerically studied in [192].

In experiments [95, 121] with collimated pulsed radiation (800 nm, 45 fs, 7 – 14 mJ), filaments were formed in air from large-scale perturbations of the initial beam profile independently of each other. However, when the pulse energy was increased up to 40 mJ, a beam consisting of many filaments was formed, which were generated at different distances from the output aperture of the laser and were irregularly arranged in the beam cross section. For such pulse parameters, intensity perturbations of transverse size ~ 0.1 cm grow with a small increment due to the modulation of instability [15]. Filaments generated from small-scale perturbations of the initial beam profile are arranged randomly and their position irregularly changes in the general case from pulse to pulse [193].

In experiments [194] on multiple filamentation with the use of the Teramobile system (100-fs, 230-μJ pulses with the peak power 700 times greater than the critical self-focusing power), first large-scale 'hot' zones were formed, which corresponded to dense multiple filaments generated in the regions of strongest fluctuations in the initial intensity distribution. At a distance of a few metres from these regions, hundreds of individual filaments appear, which are detected in the form of small-scale 'hot' dots and later occupy the entire beam cross section. According to numerical simulations [195], the number of filaments and the distance to the place of their formation are inversely proportional to the air pressure.

The formation of the multiple filamentation of radiation with the intensity perturbations in the initial beam profile was investigated in [193, 196]. From initial perturbations, the primary filaments are generated, around which ring structures caused by the defocusing of radiation in the laser plasma are formed. Due to the interference of rings diverging from closely spaced filaments, the intensity maxima appear, which become the centres of generation of 'child' filaments. Because of the energy competition between 'parental' and 'child' filaments, a part of them disappear, while filaments formed later can generate new filaments. As the distance increases, the number of filaments decreases due to energy losses and diffraction divergence reducing the energy of a reservoir supplying energy to filaments.

The stochastic nature of the formation of multiple filaments explains, in particular, the quenching of fluorescence of nitrogen molecules in plasma channels during repetitively pulsed probing of atmosphere. When initial perturbations have a higher density, a greater number of child filaments are formed, the electron density in plasma channels increases and, hence, the stability and intensity of fluorescence also increases [197, 198]. The dynamic scenario of multiple filamentation is confirmed in experiments

performed by using the high-power Extreme Light (XL)-II laser setup emitting 800-nm, 30-fs, 640-mJ pulses, which were weakly focused in air and generated dominating filaments from the initial intensity perturbations and small 'child' filaments, which decayed and merged [199]. The spatiotemporal picture of the generation and decomposition of filaments and the appearance of new filaments in a beam with large-scale harmonic intensity perturbations in the cross section obtained numerically in paper [200] was defined by the authors of this paper as optical turbulence in the pulse.

4.2 Supercontinuum of multiple filaments

The formation of a supercontinuum upon multiple filamentation is mainly determined by the spatial coherence and frequency-angular spectrum of broadband radiation generated by filaments. Femtosecond radiation has the high coherence, and supercontinuum sources appearing in the filaments of one pulse are coherent [137, 201]. The sources of the long-wavelength components of the supercontinuum are located on the axes of filaments, and the spatial distribution of the supercontinuum in this spectral region represents a set of axially symmetric peaks with centres on the axes of corresponding filaments. In the short-wavelength region, the interference of the conic emission rings of the supercontinuum diverging from each of the filaments is observed [196]. The interference pattern in a beam consisting of multiple randomly arranged filaments acquires a fancy view, its size increasing due to the angular divergence of conic emission [32]. As the distance increases, as in the one-filament regime, the efficiency of radiation conversion to the supercontinuum increases. The broadening of the frequency spectrum of the pulse in the multiple filamentation regime and the interference of the short-wavelength wing of the supercontinuum in water were studied in [202, 203].

5. Filamentation control

Filaments are formed due to the redistribution of the radiation intensity both in space upon nonlinear refraction related to the cubic and plasma nonlinearities and in time due to self-phase modulation, dispersion and self-steeping of nonlinearity. Therefore, the two types of filamentation control are possible: the time control achieved by varying the duration and initial modulation of the pulse phase and the spatial control by varying focusing and the distributions of the radiation intensity and phase in the beam cross section.

5.1 Control by phase modulation

During filamentation the material dispersion of a medium causes the transformation of the time profile of a laser pulse and its decomposition into several peaks [204–206]. Note that the material dispersion proves to be considerable also in cases when the dispersion length of the initial laser pulse exceeds the self-focusing length by one–two orders of magnitude because the duration of individual peaks can decrease down to a few femtoseconds. The pulse 'spread' due to the group velocity dispersion reduces the efficiency of energy localisation in a filament with increasing distance.

The influence of the initial phase modulation of the pulse on the filament formation is determined by two factors [134]. The first, quasi-stationary factor is a decrease in the initial power in time slices, which is independent of the phase modulation sign. The pulse duration upon phase modulation increases, the peak power decreases, and the distance to the filament onset increases according to (4). The second, dynamic factor is the preliminary compensation of the group velocity dispersion, which depends on the phase modulation sign. In a medium with the normal dispersion, a pulse with the negative phase modulation is compressed and its peak power increases during propagation. The increase of the power in the time slices of the pulse caused by its compression in the case of negative phase modulation reduces the distance to the filament onset. This distance can be estimated from above by expression (4) with the peak power for a phase-modulated pulse.

By using the negative phase modulation, filaments produced in a collimated beam of diameter 3.8 mm were displaced along the beam axis by a distance of up to 30 m [21]. To increase the filament length at kilometre distances, the authors of [23, 24] used the preliminary compensation of the group velocity dispersion due to negative phase modulation. Different filamentation regimes for 190-mJ pulses were observed in horizontal paths in air when the pulse duration increased from 200 fs to 9.6 ps at the initial phase modulation [63, 207] (Fig. 3). In vertical paths, plasma filament channels were obtained at heights ~ 2 km for phase-modulated terawatt pulses [208]. Multiterawatt pulsed radiation (1.06 μm, 570 fs, 26 J, 32 TW) produced hundreds (up to 400) of filaments in air, and independently of the initial phase modulation, a white light source (whose position corresponds to the filament onset) was detected at the same distance (19 m). The 32-TW pulses of duration 570 fs, which were close to transform-limited pulses, produced a relatively short filamentation region, which ended already at a height of 100 m, whereas in the case of phase-modulated pulses of duration 2.1 ps (9 TW), this region was extended over a distance of 350 m from the laser source.

In the case of the negative initial phase modulation, the supercontinuum broadens and its generation efficiency increases upon filamentation in a medium with the normal dispersion [24, 25]. This is explained by the increase in the energy density in the region of nonlinear interaction due to the 'temporal focusing' of radiation. As shown in paper [134], the maximum efficiency of supercontinuum generation and the maximum distance to the filament onset and the maximum filament length were achieved when the compression length of the initially phase-modulated pulse was equal to the nonlinear focusing length or slightly exceeded it.

5.2 Large-scale control and elliptic beams

Radiation focusing, global intensity redistribution and beam scaling in the beam cross section can be used for large-scale filamentation control. A filament is generated in a focused beam in front of its waist and exists behind the geometrical focus of a lens due to refocusing at peak powers considerably exceeding P_{cr} [87]. The weak focusing of radiation by lenses with focal distances $F = 8$ and 30 m was used in experiments [22] to displace the filament generation region. The control of the distance to the filament onset by varying the angular divergence and peak power of pulsed radiation (800 nm, 30 fs, 600 mJ) was demonstrated on the Extreme Light (XL)-II complex [209] equipped with a controllable bimorph mirror to vary the angular divergence of the input beam. In [210], the angular divergence of femtosecond radiation was changed by using

a simple telescopic system of two lenses with a variable distance between them.

The combined influence of focusing and initial phase modulation of a pulse on the efficiency of supercontinuum generation in air was studied numerically in [211]. It was shown that in the case of the optimal control of temporal and spatial focusing of radiation, the energy of anti-Stokes components in the pulse spectrum could achieve 5 % of the pulse energy. The possibility of the spatiotemporal control of filamentation and generation of a supercontinuum during the propagation of radiation at two different wavelengths was considered in [212]. If the power of each of the pulses is insufficient to produce filaments, a filament can be generated at a given distance when pulses are overlapped, their overlap being determined by the group velocity dispersion and time delay.

The filament parameters can be controlled by scaling the laser beam diameter and using the elliptic intensity distribution in the beam cross section. As the initial radius a of the laser beam is increased, the distance $z_{\rm fil}$ to the filament onset increases according to expression (4). When the initial beam is compressed, the linear electron density in plasma channels upon multiple filamentation increases and the stability of a fluorescence signal during femtosecond probing of air improves [213]. The increase in the axial ratio of the elliptic intensity distribution in the beam cross section leads to the increase in the critical self-focusing power and diffraction length of the beam, resulting in the increase in the distance to the filament onset [105, 106]. In addition, the ellipticity of the initial beam profile stabilise the position of filaments despite the presence of initial perturbations in the beam [214, 215]. The possibility of generating two spatially separated filaments in radiation with the astigmatic wave front was considered in [216].

5.3 Formation of an ordered group of filaments

Methods for formation of an ordered group of numerous filaments for pulses of power exceeding the critical self-focusing power by hundreds times have been developed in a number of papers. The authors of [216] proposed to produce strong gradients of a light field in the beam cross section by the overlap of masks with few holes and circular apertures. For radiation with the super-Gaussian transverse intensity distribution, a ring is formed, which decomposes due to random fluctuations into a group of filaments irregularly arranged on this ring [217].

The general approach to the spatial regularisation of a group of filaments by means of the regular modulation of the light-field amplitude or phase in the beam cross section was developed in [218, 219]. It was shown experimentally and numerically that the periodic intensity modulation can suppress stochastic filamentation caused by random fluctuations of the transverse intensity profile. Statistical calculations [220] have shown that the maximum efficiency of the spatial regularisation of a group of filaments is achieved in the case of transverse periodic intensity modulation when the radiation power corresponding to one modulation period exceeds the critical self-focusing power in a medium by a factor of 3.1 – 3.2. The method of periodic modulation of the pulse intensity with the help of a network was used in [221] for the formation of the ordered group of channels with the modified refractive index in fused silica induced by the plasma of multiple filaments.

The phase modulation of the light field in the beam cross section, unlike the amplitude modulation, does not introduce losses and is preferable for high-power radiation. The regularisation of numerous filaments by means of a phase mask was performed in [222], by means of spiral phase plates simulating wave-front dislocations – in [223], and with the help of a set of lenses tilted to the optical axis by using a bean with the elliptic profile – in [224]. The optical control of multiple filamentation by means of microlenses formed in the nonlinear-optical interaction of two overlapping radiation beams was demonstrated in [225]. By using a network modulating the transverse intensity distribution in one of the beams, a set of microlenses of diameter 500 μm with a focal distance of 37 mm was formed in a VK7 glass, which was controlled by varying the delay time of overlapped pulses. The possibility of using a lens set for the spatial regularisation of a stochastic beam of filaments produced during the propagation of a pulse in the turbulent atmosphere was numerically considered in [226].

6. Theoretical filamentation models

6.1 Nonlinear equation for a pulse envelope

In theoretical studies of filamentation the method of slowly varying amplitudes is commonly used, which is applied if the pulse envelope contains more than ten optical oscillations [150]*.

Because of the dispersion of the Kerr nonlinearity, the steepness of the trailing edge of a pulse increases during filamentation and an envelope shock wave appears [150]. In this case, the standard approach to the slowly varying amplitude equation, the so-called nonlinear Schrödinger equation, in which the terms of the first-order smallness are retained, is not valid for the description of this effect. In [227], an approach was developed which allows one to reproduce the increase in the pulse-front steepness, the appearance of the envelope shock wave, and the related extreme broadening of the pulse spectrum. Within the framework of this approach, which the authors of [227] called the slowly varying wave approximation, the equation for the envelope was obtained, which extends the region of applicability of the slowly varying amplitude method to pulsed radiation with the spectral width comparable with the carrier frequency and duration comparable with the optical oscillation cycle. For a problem of a femtosecond laser pulse filamentation, the equation for the pulse envelope $E(x, y, z, t)$ in this approximation has the form [148, 151, 228 – 230]

$$2{\rm i}k\frac{\partial E}{\partial z} = \left(1 - \frac{\rm i}{\omega}\frac{\partial}{\partial t}\right)^{-1}\Delta_\perp E - k\frac{\partial^2 k}{\partial\omega^2}\frac{\partial^2 E}{\partial t^2} + \frac{\rm i}{3}k\frac{\partial^3 k}{\partial\omega^3}\frac{\partial^3 E}{\partial t^3} + \frac{2k^2}{n_0}\left[\left(1 - \frac{\rm i}{\omega}\frac{\partial}{\partial t}\right)\Delta n_{\rm K} + \left(1 + \frac{\rm i}{\omega}\frac{\partial}{\partial t}\right)\Delta n_{\rm p}\right]E - {\rm i}k\alpha E, \quad (6)$$

where α is the absorption coefficient. The first term in the right-hand side of equation (6) describes the beam

*It is shown in [227] that this method can be applied for pulses containing down to 1.5 optical oscillations.

diffraction, the second and third terms describe the dispersion of laser radiation, the fourth term describes the change in the refractive index of the medium caused by the Kerr and plasma nonlinearities and, finally, the fifth term describes the absorption of radiation caused by the nonlinear ionisation of the medium by laser radiation. Equation (6), unlike the traditional slowly varying amplitude equation, contains the operator $[1 \pm (\mathrm{i}/\omega)(\partial/\partial t)]$, which appears when higher-order-smallness terms are retained in the expansion. A comparison of the results of numerical simulation of filamentation based on the wave equation, which directly follows from the Maxwell system of equations, and in the slowly varying wave approximation showed that supercontinuum spectra obtained by these two methods coincide in a broad wavelength range and noticeable differ only in the frequency region above 3.5ω [231].

A similar equation describing the material dispersion of a medium according to the Sellmeyer formula, was obtained in [232] for analysis of the spatial and spectral-temporal transformation of femtosecond radiation tightly focused into fused silica. Different variants of equations for a pulse envelope in the unidirectional propagation approximation were considered in [223]. For light pulses containing a few optical cycles, the equation for the strength of the electric field strength oscillating at an optical frequency was obtained [234, 235], which can be considered as the generalisation of different modifications of the equation for the pulse envelope. This approach was used to study the spatial dynamics of the light field, the formation of the blue wing of the supercontinuum during the propagation of a pulse containing a few optical cycles in a transparent dielectric, and the interaction of co-propagating and counterpropagating ultrashort pulses [236–238].

Slowly varying wave equation (6), which correctly describes a change in the profile of a pulse upon filamentation, is used fist of all for studying a decrease in the pulse duration, the transformation of its frequency spectrum, the generation of harmonics, and supercontinuum formation. In problems devoted to analysis of the spatial structure of a filament, which does not depend considerably on the increase in the pulse front steepness, the nonlinear Schrödinger equation can be applied, which is obtained from equation (6) by replacing the operator $[1 \pm (\mathrm{i}/\omega)(\partial/\partial t)]$ by unity.

The nonstationary nonlinear equation describing the filamentation of femtosecond radiation has in the general case the dimensionality $3\mathrm{D}+1$, and its solution involves considerable computational problems. To overcome these problems, splitting algorithms, schemes with nonuniform computational networks and the adaptive integration step over the evolution coordinate, and other methods are used, which increase the efficiency of numerical analysis [106, 239, 240]. The variational method [241] was applied to the problem of radiation filamentation in [242]. The equation for the effective radius of a laser beam upon filamentation was obtained in [243], where the evolution of the beam parameters in the one-filament regime was qualitatively analysed.

6.2 Plasma generation models

The change in the refractive index Δn_p caused by the generation of laser plasma due to photoionisation [244] is described in the most general form by the expression

$$\Delta n_\mathrm{p}(x,y,z,t) = -\frac{\omega_\mathrm{p}^2(x,y,z,t)}{2n_0[\omega^2+\nu_\mathrm{c}^2(x,y,z,t)]} \times\left[1-\mathrm{i}\frac{\nu_\mathrm{c}(x,y,z,t)}{\omega}\right]. \quad (7)$$

The effective frequency $\nu_\mathrm{c} = N_0 v_\mathrm{e}\sigma_\mathrm{c}$ of elastic collisions of plasma electrons with atoms and molecules is determined by the root-mean-square electron velocity $v_\mathrm{e} = eE/(m_\mathrm{e}\omega)$, the electron collision cross section σ_c, and the concentration N_0 of neutral particles. The rate ν_i of avalanche ionisation, which causes the exponential increase in the electron density in plasma, is desctibed by the expression

$$\nu_\mathrm{i} = \frac{1}{W}\frac{e^2E^2}{2m_\mathrm{e}(\omega^2+\nu_\mathrm{c}^2)}\nu_\mathrm{c}, \quad (8)$$

where W is the ionisation potential for gases or the energy band gap for condensed media.

The effective collision frequency ν_c in gases with the atmospheric density ($N_0 \approx 10^{19}$ cm^{-3}) is much lower than the optical frequency ω, the concentration N_e of plasma electrons in a filament is three orders of magnitude lower than that of neutral molecules ($N_\mathrm{e}/N_0 \leqslant 10^{-3}$), and the contribution of avalanche ionisation to the generation of electrons is negligible. In this approximation, expression (7) for the increment of the refractive index caused by the laser plasma is described by expression (2), and the term $\nu_\mathrm{i}N_\mathrm{e}$ describing avalanche ionisation in the right-hand side of kinetic equation (3) disappears.

The generation rate of electrons $R(I)$ is determined by the probability of multiphoton and tunnelling ionisation of neutral atoms and molecules in a strong light field [86], which depends, according to the Keldysh theory [85], on the adiabatic parameter $\gamma = (\omega\sqrt{2m_\mathrm{e}W}/(eE)$. The low light field strength E, at which $\gamma \gg 1$, corresponds to multiphoton ionisation, while the high strength E, at which $\gamma \ll 1$, corresponds to tunnelling ionisation. The ionisation potentials of the oxygen and nitrogen molecules are 12.1 and 15.6 eV, respectively, while the multiphoton orders K for these molecules for radiation at 800 nm are 8 and 11, respectively. In the case of multiphoton ionisation, the electron generation rate $R(I)$ is described by the power dependence $R(I) = \sigma_K I^K$. The coefficient σ_K decreases with increasing K. Thus, for oxygen, we have $\sigma_{K=8} = 2.8\times 10^{-96}$ s^{-1} cm^{16} W^{-8}, while for nitrogen, we have $\sigma_{K=11} = 6\times 10^{-140}$ s^{-1} cm^{22} W^{-11} [3].

In a filament produced by the near-IR radiation, the parameter γ for the gas components of air is close to unity, and asymptotic estimates of the ionisation rate cannot be used in this case. The photoionisation rate of nitrogen and oxygen molecules irradiated by laser pulses at 800 nm was measured in [245]. It was shown in this paper that the Perelomov–Popov–Terent'ev model [246] with the phenomenologically determined effective charge Z_eff of a molecular ion better describes experimental data than the Amosov–Delone–Krainov [247] and Szoke et al. [248] models for radiation intensities in the range from 10^{13} to 10^{15} W cm^{-2}.

A change in the electron density in the filament plasma in condensed media is determined by the filed and avalanche ionisations, which are described by kinetic equations (3). The energy gap is a few electron-volts, the filament radiation

intensity does not exceed 10^{13} W cm^{-2}, and the field-induced electronic transition from the valence band to the conduction band is mainly caused by the multiphoton process [116, 249]. For example, the energy gap for fused silica is $W = 7.6$ eV, the multiphoton order is $K = 5$ for radiation at 800 nm, and $\sigma_{K=5} = 1.3\times\ 10^{-55}$ s^{-1} cm^{10} W^{-5} [116]. The model of multiphoton field ionisation is commonly used for numerical simulations of filamentation in condensed media (see, for example, [116, 136, 250]). At the same time, according to [251], during filamentation of radiation at 800 nm, the field ionisation of fused silica is determined both by multiphoton and tunnelling processes. In [252], a model of avalanche ionisation in transparent condensed media is proposed, which involves a sequence of elementary kinetic processes of the interaction of an intense light field with free electrons terminating by impact ionisation.

7. Filamentation in atmosphere

Filamentation of femtosecond laser radiation in the real atmosphere as a multicomponent medium encompasses a broad scope of problems. One of them is the stochastic multiple filamentation of terawatt radiation, which can be caused by fluctuations of the refractive index in the turbulent atmosphere and the scattering and absorption of radiation by atmospheric aerosol particles.

7.1 Influence of atmospheric turbulence

Fluctuations of the refractive index in the atmosphere are responsible for the random nature of generation of filaments and their random walk. It was found in theoretical and experimental studies with 800-nm, 190-fs, 4.6-mJ pulses (the laser beam diameter was 9.6 mm) that random displacements of filaments in the beam cross section were isotropic and their distribution was described by the Rayleigh law [253, 254]. The average displacements of a filament in the beam cross section were 0.5 and 1.3 mm at distances 30 and 100 m, respectively.

Random fluctuations of the refractive index of air in the atmosphere initiate the stochastic decomposition of the beam into multiple filaments at peak radiation powers $P_0 \gg P_{cr}$. Phase fluctuations of the light field caused by the turbulence are transformed to intensity fluctuations and play, along with initial fluctuations, the 'seeding' role for generating multiple filaments. As a result, multiple filaments are formed, which are randomly arranged in the laser beam cross section and are generated at different distances from the output aperture of the laser system. In this case, the generation, formation, and statistic characteristics of the filament beam considerably depend on the atmospheric turbulence parameters [255].

It was found in [256] that the probability of filament formation decreased with increasing the structural constant C_n^2 of the turbulence in a layer located in front of the filament. The layers of turbulent air close to the output aperture strongly affect the formation of filaments because generated filaments weakly depend on fluctuations of the refractive index in the atmosphere [257]. Laboratory experiments [257] on the filamentation of focused 200-fs, 30-GW laser pulses in an extended turbulent layer showed that the collapse of filaments can occur only at very strong fluctuations, which are equivalent to fluctuations in an atmospheric path of length 4 km in the case of a strong turbulence with the structural constant $C_n^2 = 0.5 \times 10^{-14}$ cm$^{-2/3}$. By comparing the characteristic dimensions of spatial inhomogeneities of atmosphere and radiation, we can conclude [259] that the same fluctuations in air are small-scale at the initial stage of generation of filaments and are large-scale for filaments that were already formed. Therefore, turbulence strongly affects filaments in the process of their generation and weakly affects generated filaments, which was confirmed experimentally [258].

For pulses with the peak power slightly exceeding the critical self-focusing power, the distance to the filament onset in a path with a weak turbulence ($C_n^2 \approx 10^{-16}$ cm$^{-2/3}$) can increase compared to that in a regular medium [260, 261]. This occurs when fluctuations of the refractive index cause only small variations in the initially Gaussian intensity distribution in the beam cross section and, hence, the increase in the distance to the region of separation of the Townes mode in the beam (see section 2 of this paper) or the appearance of closely spaced perturbations, between which energy competition begins, resulting in the slowing down of the development of both filaments [191, 193]. In the case of strong enough turbulent fluctuations, the number of filaments and the average distance to the onset of the first filament decreases, while in some pulses this filament need not be formed at all [260].

As the peak intensity of input radiation was increased, the picture of formation of filaments was complicated. The interference of the light field, diverging during defocusing in the filament plasma, with the field perturbed by turbulence produces randomly arranged centres of generation of 'child' filaments [191, 240, 262]. As the structural constant C_n^2 increases, a beam of randomly formed filaments expands.

7.2 Scattering by aerosol particles

It was found in the first experiment on filamentation of laser radiation (150-fs, 2.50-TW laser pulses with the laser beam diameter 3 cm) performed in a real atmospheric path that filaments could be formed during weak rain, and the formation of diffraction rings upon scattering of pulses by water particles was observed [263]. Numerical studies [264] based on the stratified model of filamentation [265] taking into account the coherent scattering of radiation in a dispersion medium confirmed experimental results. The existence of regimes of single or multiple filamentation depending on the concentration and size of water aerosol particles was determined by the Monte-Carlo method [266].

Laboratory experiments on filamentation of laser radiation in the atmospheric aerosol [99, 267 – 269] showed that in an aerodispesion medium with a high concentration of water particles (10^5 cm^{-3}) the pulse energy and, hence, the number of filaments decreases due to scattering. This is confirmed by numerical analysis performed by replacing aerosols by a continuous absorbing medium [270].

Experiments on the interaction of a filament with separately located water drops of diameter from 30 to 100 μm showed that a 'large' particle of size comparable with the filament diameter exerts a negligible effect on the further filamentation process, which is explained by the existence of the energy reservoir maintaining filamentation (see section 2). The influence of an individual drop on a filament was considered theoretically in the simplest model approximation by simulating a particle by an absorbing disc [271].

7.3 Filamentation at a distance of a few kilometres

The formation of filaments at large distances from a laser system, for example, a few kilometres is very important for atmospheric applications. One of the methods for increasing a distance to the region of formation of filaments is beam scaling [272]. The increase in the beam cross section and the spatial scale of its inhomogeneities inhibits the development of small-scale focusing and, therefore, stochastic filamentation. In the case of long atmospheric paths, the most efficient is a combination of the laser beam scaling, its focusing, and initial phase modulation. It was shown numerically [273, 274] that the negative phase modulation not only displaced the filament onset in air but also can change the type of refocusing, by increasing the length of the filamentation region, whereas the continuity of a filament plasma channel can be controlled by beam focusing [275]. To calculate approximately the filamentation of phase-modulated pulsed radiation at distances of a few kilometres, a semi-analytic model was proposed [276], which takes into account the influence of turbulent fluctuations of the refractive index on the development of multiple filamentation at atmospheric paths.

7.4 Filamentation at high altitudes

The properties of filamentation of femtosecond radiation at high altitudes and vertical atmospheric paths are determined by the dependence of the air density of the altitude and increase in the critical self-focusing power with increasing altitude. In a vertical path, filaments are formed at a larger distance than in a horizontal path, and their number decreases during multiple filamentation. This is confirmed by experiments performed in [263] at a horizontal path of length 325 m at an altitude of 3.2 km over the sea level. It was shown experimentally and theoretically [277] that the radiation intensity in a filament is independent of the air pressure and, hence, its diameter increases with altitude. It was found experimentally [278] that, as a pressure decreased from 1 to 0.2 atm, the peak conduction of a plasma filament channel remained constant but its length decreased approximately by a factor of 1.5. It was shown numerically in [279] that, by using phase-modulated pulses, the filament onset in vertical paths can be displaced up to an altitude of 6.8 km.

8. Application of filamentation in atmospheric optics

8.1 Probing of the environment. A femtosecond lidar

Supercontinuum emission generated by femtosecond laser radiation upon filamentation can be used for probing the environment [5, 22, 24, 280]. First, this pulsed radiation, appearing due to nonlinear-optical transformation, has the femtosecond duration, which provides a high spatial resolution. Second, it has a broad spectrum covering the absorption lines of many pollutants and such gases as ozone, benzene and toluene vapours, etc. [25]. Thus, the supercontinuum of a filament provides the broadband spectral-temporal analysis of the multifrequency response of a medium under study with a high spatial resolution. Compared to a differential absorption two-wave lidar, no problems occur when a femtosecond lidar is used to probe narrow absorption lines such as, for example, water absorption lines [23]. The width of the continuum spectrum upon filamentation considerably exceeds, for example, the spectral range of a tunable OPO lidar [281]. The angular distribution of supercontinuum scattering can give information on the size of drops and their concentration inside a cloud layer being probed [282].

Time-resolved visible and IR absorption spectra were obtained by using the supercontinuum emission produced upon filamentation of terawatt femtosecond radiation [283]. The absorption lines of water vapour recorded in these experiments coincide with the known spectroscopic data, and their recording in the band of width 200 nm allows one to measure simultaneously the air temperature and the water vapour concentration. The possibility to move a supercontinuum source (filament) closer to an object being probed [208] and the existence of large local gradients of the refractive index induced by the filament [284] increase the level of the detected signal.

Note that the intense radiation of filaments produces the dissociation and multiphoton excitation of pollutant molecules. The characteristic lines of this fluorescence also can be used for the remote diagnostics of the concentration of pollutants, which provides the additional probing channel [4].

8.2 Fluorescence and emission spectroscopy induced by filaments

Laser-induced breakdown spectroscopy uses fluorescence emission appearing in the optical breakdown plasma produced by a high-power laser pulse. The threshold of a target ablation accompanying the optical surface breakdown is $\sim 120 - 180$ mJ cm^{-2} for copper [285, 286], which is an order of magnitude lower than the energy density ~ 1 J cm^{-2} in a femtosecond filament. Thus, high-power femtosecond laser pulses in the filamentation regime can be used to deliver energy for producing the optical breakdown plasma and a fluorescence signal from targets located at distances of a few kilometres. This method is called the filament-induced breakdown spectroscopy (FIBS). In the case of multiple filamentation of multiterawatt laser radiation, the fluorescence signal increases due to the summation of contributions from sources initiated on a target by each filament.

The first FIBS experiments with remote metal targets in atmosphere were performed in [29, 58] and later in [287, 288]. It follows from the results obtained for a target located at a distance of 180 m from a laser (emitting 795-nm, 75-fs, 350-mJ pulses at a repetition rate of 10 Hz) that, to obtain the maximum fluorescence intensity, it is necessary to produce filaments at a distance of a few metres from the target [58]. In this case, the maximum probing distance providing the resolution of atomic copper lines with the use of a ICCD camera for detection was 150 m [29, 58]. The estimates presented in [288] show that, by using terawatt laser systems for probing at distances ~ 1 km, it is possible to obtain a FIBS signal sufficient for diagnostics of metal targets even for one pulse. The FIBS diagnostics used in the lidar measuring scheme can be performed at distances up to a few kilometres [58]. In this case, the limiting factor is not a detecting system but a distance at which filamentation occurs, i.e. the possibility of obtaining filamentation at large distances.

The remote diagnostics of various metals and minerals by FIBS spectroscopy was first performed in [289] with the

help of filaments produced by using 248-nm, 450-fs, 20-mJ laser pulses. The remote FIBS detection of biological aerosols in atmosphere was demonstrated in [290 – 292].

8.3 Control of a high-voltage discharge

One of the possible applications of conducting plasma filament channels can be the creation of a controllable electric discharge, in particular, for controlling thunder lightnings [24]. The main motivation in this case is the protection of vital objects from lightning discharges.

A discharge was initiated by a filament in laboratory experiments [293 – 295] by coupling radiation from a femtosecond laser through a hole at the centre of flat electrodes into a gap between them. The gap width was 2 – 4.5 m, and a voltage of a few megavolts was applied across the electrodes. When filaments appeared between electrodes, a conducting discharge channel became regular and reproducible, the breakdown threshold decreased by 30 % and the development time of the controllable discharge decreased. The possibility of increasing the control efficiency with the help of the second 'maintaining' nanosecond pulse of energy a few hundreds of millijoules was demonstrated in [296].

It was shown in [30] that, unlike the tight focusing of a laser beam, in the case of filamentation the main 'triggering' mechanism of a discharge is the joule heating of air in a filament channel followed by the production of a low pressure in the filament, which is accompanied by the corresponding decrease in the breakdown threshold. In [297], a beam of plasma channels was used to obtain a continuous discharge of duration above 1 s between two electrodes to which constant or alternate 50-Hz voltage was applied. The temporal and spatial dynamics of a breakdown initiated by filaments studied in [298] revealed the appearance of two different breakdown regimes: the 'slow' regime with the characteristic time of the order of a millisecond and the 'fast' regime with the characteristic time about a few microseconds, at which the breakdown threshold decreased by 40 %.

Laboratory experiments simulating the control of a high-voltage discharge in a dense water cloud were performed in [299], and full-scale experiments during raining were performed in [300]. During the formation of a beam of filaments of length ~ 100 m by radiation from a terawatt laser system located at an altitude of 3209 m over the seal level, radiofrequency pulses were detected which were produced in electric processes in thunderclouds synchronised with the formation of filaments.

8.4 Dynamic microwave waveguides

The plasma channel of a filament is a thin current-conducting thread with an instant length of 1 – 3 m, which 'flies' together with the laser pulse over tens and hundreds of metres. Such a dynamic filament can be treated as a virtual line for the directional transfer of the electromagnetic energy [301]. The formation dynamics of a virtual cylindrical waveguide consisting of plasma channels of multiple filaments, the possibility of increasing its effective thickness due to the formation of a multilayer structure and the estimates of the main waveguide parameters for microwave radiation were considered in [302].

In the experiment confirming the above-mentioned idea, a virtual plasma waveguide of diameter 4.5 cm was formed by more than a thousand of plasma channels, which were produced by using pulsed radiation (800-nm, 27-fs, 1.5-J, 100-TW pulses) focused to a ring by a flexible deformable mirror [303]. An increase in the microwave emission signal at a wavelength of 3 cm was detected at a distance of 16 cm at the instants of formation of a virtual waveguide. The possibility of obtaining a dielectric waveguide from plasma filament channels was discussed in [304].

9. Application of filamentation in the development of microoptics elements

A high power density of femtosecond radiation allows the photoinduced micromodification of optical materials without their thermal damage. The application of near-IR radiation for changing the refractive index of optical materials was first demonstrated in [31]. Radiation focused near a sample surface produced a thermal shock resulting in the damage of the surface, whereas radiation focused into the sample caused a change in the refractive index of the material at the focal spot without damage at energy densities up to 100 mJ cm^{-2}. Micromodification lines were recorded by moving the sample at rates of 0.1 – 10 mm s^{-1} perpendicular and parallel to the laser beam (Fig. 11).

9.1 Micromodification of optical materials

The main experiments were performed by scanning samples exposed to the 800-nm radiation tightly focused inside them. As the exposure was increased due to the increase in the pulse energy or decrease in the scanning rate of a sample, the increment Δn of the refractive index saturated, achieving 3×10^{-3} in pure quartz and 5×10^{-3} in quartz doped with boron [305]. For the pulse energy density of 8 – 10 J cm^{-2}, the increment Δn was 3×10^{-4}, while the increment of the material density was ~ 0.1 %, which is equivalent to the change in the quartz temperature by 500 °C. When the pulse energy density was increased up to 40 J cm^{-2}, the increment Δn achieved 500×10^{-4} and the density increment was ~ 11 %, which corresponds to the action of a strongly localised shock wave with the amplitude 26×10^9 Pa appearing during the relaxation of the laser plasma energy in an atomic lattice [306].

The measurement of the energy of the delayed probe radiation scattered in the modified region produced by 800-nm, 110-fs pulses at a repetition rate of 1 kHz showed that the time of plasma formation and structural changes in a material was ~ 35 ps [307]. The electron density in the laser plasma and the electron collision time measured by time-resolved shadow and interferometric methods were 5×10^{19} cm^{-3} and 1.7 fs, respectively [308]. A change in the cubic susceptibility in the induced micromodification channel was studied in [309].

The existence of different micromodification regimes in fused silica and the appearance of a birefringent region were found in [310]. The first irreversible modification of a material with $\Delta n = 5 \times 10^{-3}$ is isotropic and can be annealed at a temperature of 600 °C, while the second modification with $\Delta n = 10^{-2}$ corresponds to the appearance of the local birefringence and is preserved after annealing at 900 °C for a hour. Investigations performed for fused silica cleavages showed that the shear stress appears in the material [311]. The controllable variation in the refractive index in fused silica appears upon irradiation by 0.35 – 1.5-μJ pulses of durations from 130 to 230 fs [312]. The

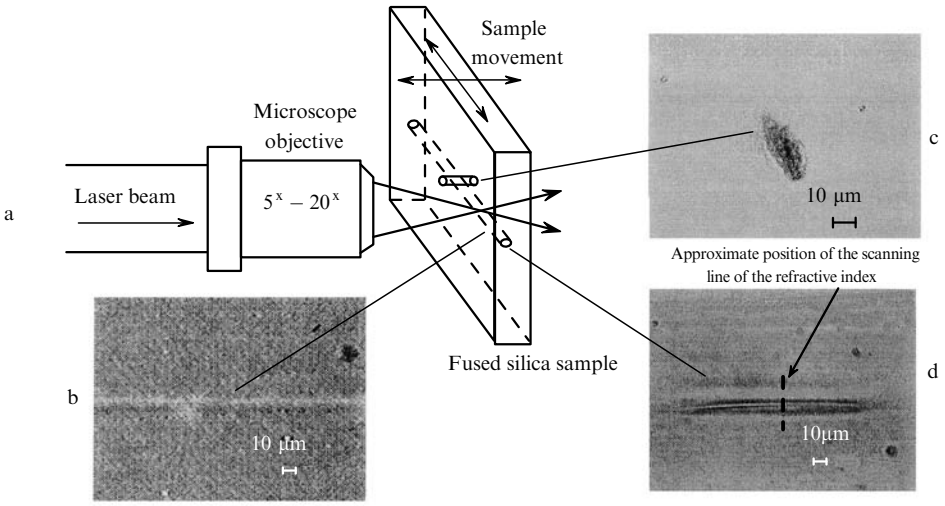

Figure 11. Scheme for recording micromodifications in an optical material by femtosecond laser radiation (a); the side view of a waveguide obtained by moving a sample in a plane perpendicular to the pulse propagation direction (b); and images of cross sections of waveguides during the longitudinal (c) and transverse movements of the sample [31].

micromodification threshold increases with decreasing the pulse duration, by forming in the pulse energy-duration plane a triangle region of admissible pulse parameters for inducing the increment $\Delta n = 2 \times 10^{-4} - 1.6 \times 10^{-3}$ in silica. The results of studies performed in [74, 312–314] allow the optimisation of laser pulse parameters for formation micromodification channels in optical materials. The application of commercial 1.55-μm fibre lasers for micromodifications of fused silica was demonstrated in [315].

In experiments on the micromodification of materials upon radiation filamentation, a sample is fixed and the transformation of an induced channel is detected by varying the exposure time, duration, energy, and polarisation of weakly focused radiation [71, 316, 317]. A micromodification channel is formed in the region of a filament and grows with increasing exposure in the direction opposite to the radiation propagation direction [71]. The channel growth saturates and its length achieves 500 μm during the exposure time of 30 min for 0.7–2.3-μJ pulses at a repetition rate of 1 kHz focused by a lens with the numerical aperture NA = 0.05. As the NA is increased, the saturation time and the channel length in silica decrease. The channel diameter, equal to 1.7 μm, and the increment of the refractive index in it, equal to 0.8×10^{-2}, remain invariable. For circularly polarised incident radiation, the cross section of the induced channel has the shape of a circle, while for linearly polarised radiation, it has the form of an ellipse with the major axis directed along the polarisation direction [316]. The change in the refractive index $\Delta n = (1.1 - 4.6) \times 10^{-4}$ in niobium–telluric glasses was obtained by moving samples parallel to the propagation direction of a femtosecond pulse [318].

The theoretical studies of changes in the optical properties of materials induced by femtosecond pulses are considerably falling behind the experimental research. The analysis of a thermal model by the examples of silica and borosilicate glass showed [319] that temperature is not a dominating factor for modification because the observed increase in the refractive index Δn can be possible only at temperatures that are not achieved in the regimes used in experiments. The estimate of structural changes produced by a shock wave during the relaxation of the laser plasma shows that the increment Δn caused by the change in the sample density is an order of magnitude lower than the measured value. The generation of colour centres by laser radiation can make a considerable contribution in the change in the refractive index. Their concentration achieves 3×10^{19} cm^{-3}, which corresponds to $\Delta n \sim 10^{-3}$. However, the annealing temperature of colour centres is significantly lower than the temperature corresponding to the induced refractive index. The general description of processes proceeding in wide-gap dielectrics irradiated by femtosecond laser pulses is presented in [249].

Micromodifications induced by filaments were used to fabricate waveguide couplers [320–322], hexagonal arrays of coupled waveguides [323], diffraction gratings [316], focusing transparencies [324], and other elements of microoptics [325].

10. Conclusions

A new direction in optics – the nonlinear optics of femtosecond filaments, developed recently, encompasses a broad scope of problems of nonlinear-optical interaction of spatiotemporally self-localised femtosecond radiation with a medium. The long-known and again enigmatic phenomenon of filamentation of laser radiation poses new questions for researchers and opens up unexpected fields of practical applications of laser physics.

Acknowledgements. This work was supported by the Russian Foundation for Basic Research (Grant Nos 08-02-00517a and 09-02-01200-a).

References

1. Kandidov V.P., Kosareva O.G., Brodyur A., Chin S.L. *Opt. Atmos. Okean.*, **10**, 966 (1997).
2. Chin S.L., Hosseini S.A., Liu W., et al. *Can. J. Phys.*, **83**, 863 (2005).
3. Couairon A., Mysyrowicz A. *Phys. Rep.*, **441**, 47 (2007).
4. Berge L., Skupin S., Nuter R., et al. *Rep. Prog. Phys.*, **70**, 1633 (2007).

5. Kasparian J., Wolf J.-P. *Opt. Express*, **16** (1), 466 (2008).
6. *Appl. Phys. B*, **77** (2003).
7. Boyd R.W., Lukishova S.G., Shen Y.R. (Eds) *Self-focusing: Past and Present. Fundamentals and Prospects* (Topics in Applied Physics; Berlin: Springer, 2008) Vol. 114.
8. Pilipetskii N.F., Rustamov A.R. *Pis'ma Zh. Eksp. Teor. Fiz.*, **2**, 88 (1965).
9. Askar'yan G.A. *Zh. Eksp. Teor. Fiz.*, **42**, 1567 (1962).
10. Chiao R.Y., Garmire E., Townes C.H. *Phys. Rev. Lett.*, **13**, 479 (1964).
11. Hercher M. *J. Opt. Soc. Am.*, **54**, 563 (1964).
12. Garmire E., Chiao R.Y., Townes C.H. *Phys. Rev. Lett.*, **16**, 347 (1966).
13. Korobkin V.V., Alcock A.J. *Phys. Rev. Lett.*, **21**, 1433 (1968).
14. Basov N.G., Kryukov P.G., Senatskii Yu.V., Chekalin S.V. *Zh. Eksp. Teor. Fiz.*, **57**, 1175 (1969).
15. 15. Bespalov V.I., Talanov V.I. *Pis'ma Zh. Eksp. Teor. Fiz.*, **3**, 471 (1966).
16. Basov N.G., Zaritskii A.R., Zakharov S.D., et al. *Kvantovaya Elektron.*, (6), 50 (1972) [*Sov. J. Quantum Electron.*, **2** (6), 533 (1972)].
17. Fleck J.A. Jr., Layne C. *Appl. Phys. Lett.*, **22**, 467 (1973).
18. Braun A., Korn G., Liu X., et al. *Opt. Lett.*, **20**, 73 (1995).
19. Nibbering E.T.J., Gurley P.F., Grillon G., et al. *Opt. Lett.*, **21**, 62 (1996).
20. Brodeur A., Kosareva O.G., Chien C.Y., et al. *Opt. Lett.*, **22**, 304 (1997).
21. La Fontaine B., Vidal F., Jiang Z., et al. *Phys. Plasmas*, **6** (5), 1615 (1999).
22. Wöste L., Wedekind C., Wille H., et al. *Laser und Optoelectronik*, **29** (5), 51 (1997).
23. Wille H., Rodriguez M., Kasparian J., et al. *Eur. Phys. J. Appl. Phys.*, **20**, 183 (2002).
24. Kasparian J., Rodriguez M., Méjean G., et al. *Science*, **301** (5629), 61 (2003).
25. Kasparian J., Sauerbrey R., Mondelain D., et al. *Opt. Lett.*, **25** (18), 1397 (2000).
26. Bejot P., Bonacina L., Extermann J., et al. *Appl. Phys. Lett.*, **90**, 151106 (2007).
27. Luo Q., Xu H.L., Hosseini S.A., et al. *Appl. Phys. B*, **82**, 105 (2006).
28. Méjean G., Kasparian J., Yu J., et al. *Appl. Phys. B*, **78**, 535 (2004).
29. Stelmaszczyk K., Rohwetter Ph., Méjean G., et al. *Appl. Phys. Lett.*, **85** (18), 3977 (2004).
30. Tzortzakis S., Prade B.S., Franco M.A., et al. *Phys. Rev. E*, **64**, 057401 (2001).
31. Davis K.M., Miura K., Sugimoto N., Hirao K. *Opt. Lett.*, **21**, 1729 (1996).
32. Liu W., Hosseini S.A., Ferland B., et al. *New J. Phys.*, **6**, 1 (2004).
33. Ting A., Gordon D.F., Briscoe E., et al. *Appl. Opt.*, **44**, 1474 (2005).
34. Fujimoto M., Aoshima S., Hosoda M., Tsuchiya Y. *Opt. Lett.*, **24**, 850 (1999); *Phys. Rev. A*, **64**, 033813 (2001).
35. Fujimoto M., Aoshima S., Tsuchiya Y. *Opt. Lett.*, **27**, 309 (2002).
36. Potenza M.A.C., Minardi S., Trull J., et al. *Opt. Commun.*, **229**, 38 (2004).
37. Matijošius A., Piskarskas R., Gaižauskas E., et al. *Nonlinear Anal.: Model. Control*, **9** (3), 259 (2004).
38. Bragheri F., Liberale C., Degiorgio V., et al. *Opt. Commun.*, **256**, 166 (2005).
39. Tzortzakis S., Franco M.A., Andre Y.-B., et al. *Phys. Rev. E*, **60**, R3505 (1999).
40. Tzortzakis S., Prade B., Franco M., Mysyrowicz A. *Opt. Commun.*, **181**, 123 (2000).
41. Gopal A., Minardi St., Tatarakis M. *Opt. Lett.*, **32**, 1238 (2007).
42. Liu J.S., Duan Z.L., Zeng Z.N., et al. *Phys. Rev. E*, **72**, 026412 (2005).
43. Deng Y.P., Zhu J.B., Ji Z.G., et al. *Opt. Lett.*, **31** (4), 546 (2006).
44. Yu J., Mondelain D., Kasparian J., et al. *Appl. Opt.*, **42**, 7117 (2003).
45. Proulx A., Talebpour A., Petit S., Chin S.L. *Opt. Commun.*, **174**, 305 (2000).
46. Bukin V.V., Garnov S.V., Malyutin A.A., Strelkov V.V. *Kvantovaya Elektron.*, **37**, 961 (2007) [*Quantum Electron.*, **37**, 961 (2007)].
47. Moll K.D., Gaeta A.L. *Phys. Rev. Lett.*, **90**, 203902 (2003).
48. Hauri C.P., Lopez-Martens R.B., Blaga C.I., et al. *Opt. Lett.*, **32**, 868 (2007).
49. Prade B., Franco M., Mysyrowicz A., et al. *Opt. Lett.*, **31**, 2601 (2006).
50. Chin S.L., Théberge F., Liu W. *Appl. Phys. B*, **86**, 477 (2007).
51. Kasparian J., Sauerbrey R., Chin S.L. *Appl. Phys. B*, **71**, 877 (2000).
52. Becker A., Akozbek N., Vijayalakshmi K., et al. *Appl. Phys. B*, **73**, 287 (2001).
53. Liu W., Petit S., Becker A., et al. *Opt. Commun.*, **202**, 189 (2002).
54. Théberge F., Liu W., Simard P.Tr., et al. *Phys. Rev. E*, **74**, 036406 (2006).
55. Schillinger H., Sauerbrey R. *Appl. Phys. B*, **68**, 753 (1999).
56. Talebpour A., Abdel-Fattah M., Chin S.L. *Opt. Commun.*, **183**, 479 (2000).
57. Chien C.Y., La Fontaine B., Desparois A., et al. *Opt. Lett.*, **25**, 578 (2000).
58. Rohwetter Ph., Stelmaszczyk K., Woste L., et al. *Spectrochim. Acta. Pt B*, **60**, 1025 (2005).
59. Yang H., Zhang J., Li Y., et al. *Phys. Rev. E*, **66**, 016406 (2002).
60. Hao Z.Q., Zhang J., Li Y.T., et al. *Appl. Phys. B*, **80**, 627 (2005).
61. Luo Q., Yu J., Hosseini S.A., et al. *Appl. Opt.*, **44** (3), 391 (2005).
62. Hui Yang, Jie Zhang, Yingjun Li, et al. *Phys. Rev. E*, **66**, 016406 (2002).
63. Mechain G., D'Amico C., Andre Y.-B., et al. *Opt. Commun.*, **247**, 171 (2005).
64. Liu W., Luo Q., Chin S.L. *Chinesse Opt. Lett.*, **1**, 56 (2003).
65. Mikalauskas D., Dubieties A., Danielus R. *Appl. Phys. B*, **75**, 899 (2001).
66. Bejot P., Bonnet C., Boutou V., Wolf J.-P. *Opt. Express*, **15**, 13295 (2007).
67. Schwarz J., Rambo P., et al. *Opt. Commun.*, **180**, 383 (2000).
68. Tzortzakis S., Lamouroux B., Chiron A., et al. *Opt. Lett.*, **25**, 1270 (2000).
69. Tzortzakis S., Lamouroux B., Chiron A., et al. *Opt. Commun.*, **197**, 131 (2001).
70. Naudeau M.L., Law R.J., Luk T.S., et al. *Opt. Express*, **14** (13), 6194 (2006).
71. Yamada K., Watanabe W., Toma T., et al. *Opt. Lett.*, **26**, 19 (2001).
72. Hiroshi Kumagai, Sung-Hak Cho, Kenichi Ishikawa, et al. *J. Opt. Soc. Am. B*, **20**, 597 (2003).
73. Sudrie L., Couairon A., Franco M., et al. *Phys. Rev. Lett.*, **89**, 186601 (2002).
74. Nguyen N.T., Saliminia A., Liu W., et al. *Opt. Lett.*, **28**, 1591 (2003).
75. Kosareva O.G., Grigor'evskii A.V., Kandidov V.P. *Kvantovaya Elektron.*, **35**, 1013 (2005) [*Quantum Electron.*, **35**, 1013 (2005)].
76. Gordienko V.M., Makarov I.A., Mikheev P.M., et al. *Proc. SPIE Int. Soc. Opt. Eng.*, **5399**, 96 (2003).
77. Chutko E.A., Gordienko V.M., Kirillov B.A., et al. *Laser Phys.*, **13**, 1102 (2003).
78. Papazoglou D.G., Zergioti I., Tzortzakis S. *Opt. Lett.*, **32**, 2055 (2007).
79. Minardi S., Gopal A., Tatarakis M., et al. *Opt. Lett.*, **33**, 86 (2008).
80. Schroeder H., Chin S.L. *Opt. Commun.*, **234**, 399 (2004).
81. Liu W., Kosareva O., Golubtsov I.S., et al. *Appl. Phys. B*, **76**, 215 (2003).
82. Dubietis A., Tamosauskas G., Diomin I., Varanavicius A. *Opt. Lett.*, **28**, 1269 (2003).
83. Dubietis A., Couairon A., Kusinskas E., et al. *Appl. Phys. B*, **84**, 439 (2006).
84. D'Amico C., Prade B., Franco M., Mysyrowicz A. *Appl. Phys. B*, **85**, 49 (2006).
85. Keldysh L.V. *Zh. Eksp. Teor. Fiz.*, **47**, 1945 (1964).

86. Delone N.B., Krainov V.P. *Nelineinaya ionizatsiya atomov lazernym izlucheniem* (Nonlinear Ionisation of Atoms by Laser Radiation) (Moscow: Fizmatlit, 2001).
87. Lange H.R., Grillon G., Ripoche J.-R., et al. *Opt. Lett.*, **23**, 120 (1998).
88. Kosareva O.G., Kandidov V.P., Brodeur A., Chin S.L. *J. Nonlinear Opt. Physics Mat.*, **6**, 485 (1997).
89. Lugovoi V.N., Prokhorov A.M. *Pis'ma Zh. Eksp. Teor. Fiz.*, **7**, 153 (1968).
90. Giuliano C.R., Marburger J.H. *Phys. Rev. Lett.*, **27**, 905 (1971).
91. Korobkin V.V., Prokhorov A.M., Serov R.V., Shchelev M.Ya. *Pis'mas Zh. Eksp. Teor. Fiz.*, **11**, 153 (1970).
92. Loy M.T., Shen Y.R. *Phys. Rev. Lett.*, **22**, 994 (1969).
93. Golubtsov I.S., Kandidov V.P., Kosareva A.G. *Opt. Atmos. Okean.*, **14**, 335 (2001).
94. Chin S.L., Akozbek N., Proulx A. *Opt. Commun.*, **188**, 181 (2001).
95. Chin S.L., Petit S., Liu W., et al. *Opt. Commun.*, **210**, 329 (2002).
96. Mlejnek M., Wright E.M., Moloney J.V. *Opt. Lett.*, **23**, 382 (1998).
97. Kandidov V.P., Kosareva O.G., Koltun A.A. *Kvantovaya Elektron.*, **33**, 69 (2003) [*Quantum Electron.*, **33**, 69 (2003)].
98. Dubietis A., Gaizauskas E., Tamosauskas G., Di Trapani P. *Phys. Rev. Lett.*, **29**, 253903 (2004).
99. Courvoisier F., Boutou V., Kasparian J., et al. *Appl. Phys. Lett.*, **83** (2), 213 (2003).
100. Liu W., Cravel J.-F., Theberge F., et al. *Appl. Phys. B*, **80**, 857 (2005).
101. Talebpour A., Petit S., Chin S.L. *Opt. Commun.*, **171**, 285 (1999).
102. Liu W., Chin S.L., Kosareva O.G., et al. *Opt. Commun.,* **225**, 193 (2003).
103. Marburger J.H. *Prog. Quant. Electr.*, **4**, 35 (1975).
104. Fibich G., Gaeta A.L. *Opt. Lett.*, **25**, 335 (2000).
105. Fibich G., Ilan B. *J. Opt. Soc. Am. B*, **17**, 1749 (1999).
106. Kandidov V.P., Fedorov V.Yu. *Kvantovaya Elektron.*, **34**, 1163 (2004) [*Quantum Electron.*, **34**, 1163 (2004)].
107. Petit S., Talebpour A., Proulx A., Chin S. *Opt. Commun.*, **175**, 323 (2000).
108. Hellwarth R.W., Pennington D.M., Henesian M.A. *Phys. Rev. A*, **41**, 2766 (1990).
109. Nibbering E.T.J., Grillon G., Franco M.A., et al. *Opt. Soc. Am. B*, **14**, 650 (1997).
110. Liu W., Chin S.L. *Opt. Express*, **13**, 5750 (2005).
111. Mizrahi V., Shelton D.P. *Phys. Rev. Lett.*, **55**, 696 (1985).
112. Fedorov V.Yu., Kandidov V.P. *Opt. Spektrosk.*, **105**, 291 (2008).
113. Auston D.H., in *Ultrashort Light Pulses* (Berlin: Springer, 1977).
114. Brodeur A., Chin S.L. *Phys. Rev. Lett.*, **80**, 4406 (1998).
115. Smith W.L., Liu P., Bloembergen N. *Phys. Rev. A*, **15**, 2396 (1977).
116. Tzortzakis S., Sudrie L., Franco M., et al. *Phys. Rev. Lett.*, **87**, 213902 (2001).
117. Hellwarth R., Cherlow J., Yang T.-T. *Phys. Rev. B*, **11**, 964 (1975).
118. Oleinikov P.A., Platonenko V.T. *Laser Phys.*, **3**, 618 (1993).
119. Ripoche J.-F., Grillon G., Prade B., et al. *Opt. Commun.*, **135**, 310 (1997).
120. Chiron A., Lamoroux B., Lange R., et al. *Eur. Phys. J. D*, **6**, 383 (1999).
121. Andrianov K.Yu., Kandidov V.P., Kosareva O.G., et al. *Izv. Ross. Akad. Nauk, Ser. Fiz.*, **66**, 1091 (2002).
122. Babin A.A., Kartashov D.V., Kiselev A.M., et al. *Appl. Phys. B*, **75**, 509 (2002).
123. Ranka J.K., Windeler R.S., Stentz A.J. *Opt. Lett.*, **25**, 25 (2000).
124. Fedotov A.B., Zheltikov A.M., Tarasevitch A.P., von der Linde D. *Appl. Phys. B*, **73**, 181 (2001).
125. Shimizu F. *Phys. Rev. Lett.*, **19**, 1097 (1967).
126. Gustafson T.K., Taran J.P., Haus H.A., et al. *Phys. Rev.*, **177**, 306 (1969).
127. Alfano R.R., Shapiro S.L. *Phys. Rev. Lett.*, **24**, 592 (1970).
128. Alfano R.R., Hope L.L., Shapiro S.L. *Phys. Rev. A*, **6**, 433 (1972).
129. Nishioka H.,. Odajima W., Ueda K., Takuma H. *Opt. Lett.*, **20**, 2505 (1995).
130. Trushin S.A., Panja S., Kosma K., et al. *Appl. Phys. B*, **80**, 399 (2005).
131. Bejot P., Kasparian J., Salmon E., et al. *Appl. Phys. B*, **87**, 1 (2007).
132. Hui Yang, Jie Zhang, Qiuju Zhang, et al. *Opt. Lett.*, **30**, 534 (2005).
133. Skupin S., Berge L. *Opt. Commun.*, **280**, 173 (2007).
134. Golubtsov I.S., Kandidov V.P., Kosareva O.G. *Kvantovaya Elektron.*, **33**, 525 (2003) [*Quantum Electron.*, **33**, 525 (2003)].
135. Méjean G., Kasparian J., Salmon E., et al. *Appl. Phys. B*, **77**, 357 (2003).
136. Kolesik M., Katona G., Moloney J.V., Wright E.M. *Phys. Rev. Lett.*, **91**, 043905 (2003).
137. Chin S.L., Brodeur A., Petit S., et al. *J. Nonlinear Opt. Physics Mat.*, **8**, 121 (1999).
138. Nagura Ch., Suda A., Kawano H., et al. *Appl. Opt.*, **41**, 3735 (2002).
139. Dharmadhikari A.K., Rajgara F.A., Reddy N.C., et al. *Opt. Express*, **12**, 695 (2004).
140. Dharmadhikari A.K., Rajgara F.A., Mathur D. *Appl. Phys. B*, **80**, 61 (2005); **82**, 575 (2006).
141. Corkum P.B., Rolland C., in *Atomic and Molecular Processes with Short Intense Laser Pulses*. (NATO ASI Ser. Phys. B; New York: Plenum Press, 1987) Vol. 171, p. 157.
142. Siders C.W., Turner N.C., Downer M.C., et al. *J. Opt. Soc. Am. B*, **13**, 330 (1996).
143. Golub I. *Opt. Lett.*, **15**, 305 (1990).
144. Xing Q., Yoo K.M., Alfano R.R. *Appl. Opt.*, **32**, 2087 (1993).
145. Grenshaw M.E., Cantrell C.D. *Phys. Rev. A*, **39**, 126 (1989).
146. Rae S.C. *Opt. Commun.*, **104**, 330 (1994).
147. Kosareva O.G., Kandidov V.P., Brodeur A., et al. *Opt. Lett.*, **22**, 1332 (1997).
148. Golubtsov I.S., Kosareva O.G. *Opt. Zh.*, **69**, 21 (2002).
149. Faccio D., Porras M.A., Dubietis A., et al. *Opt. Commun.*, **265**, 672677 (2006).
150. Akhmanov S.A., Vysloukh V.A., Chirkin A.S. *Optika femtosekundnykh lazernykh impul'sov* (Optics of Femtosecond Laser Pulses) (Moscow: Nauka, 1988).
151. Kandidov V.P., Kosareva O.G., Golubtsov I.S., et al. *Appl. Phys. B*, **77**, 149 (2003).
152. Gaeta A.L. *Phys. Rev. Lett.*, **84**, 3582 (2000).
153. Trushin S.A., Kosma K., Fuβ W., Schmid W.E. *Opt. Lett.,* **32**, 2432 (2007).
154. Golubtsov I.S., Kandidov V.P., Kosareva O.G. *Kvantovaya Elektron.*, **34**, 348 (2004) [*Quantum Electron.*, **34**, 348 (2004)].
155. Gaižauskas E., Vanagas E., Jarutis V., et al. *Opt. Lett.*, **31**, 80 (2006).
156. Kompanets V.O., Chekalin S.V., Kosareva O.G., et al. *Kvantovaya Elektron.*, **36**, 821 (2006) [*Quantum Electron.*, **36**, 821 (2006)].
157. Couairon A., Gaižauskas E., Faccio D., et al. *Phys. Rev. E*, **73**, 016608 (2006).
158. Conti C., Trillo S., Di Trapani P., et al. *Phys. Rev. Lett.*, **90**, 170406 (2003).
159. Faccio D., Matijosius A., Dubietis A., et al. *Phys. Rev. E*, **72**, 037601 (2005).
160. Faccio D., Averchi A., Lotti A., et al. *Opt. Express*, **16**, 1565 (2008).
161. Faccio D., Porras M., Dubietis A., et al. *Phys. Rev. Lett.*, **96**, 193901 (2006).
162. Kolesik M., Wright E.M., Moloney J.V. *Opt. Express*, **13**, 10729 (2005).
163. Faccio D., Averchi A., Couairon A., et al. *Opt. Express*, **15**, 13077 (2007).
164. Moll K.D., Gaeta A. *Opt. Lett.*, **29**, 995 (2004).
165. Berge L., Skupin S. *Phys. Rev. E*, **71**, 065601 (2005).
166. Porras M.A., Dubietis A., Matijošius A., et al. *J. Opt. Soc. Am. B*, **24**, 581 (2007).
167. Fedotov A.B., Koroteev N.I., Loy M.M.T., et al. *Opt. Commun.*, **133**, 587 (1997).

168. Akozbek N., Iwasaki A., Becker A., et al. *Phys. Rev. Lett.*, **89** (14), 143901 (2002).
169. Yang H., Zhang J., et al. *Phys. Rev. E*, **67** (1), 015401 (2003).
170. Peatross J., Backus S., Zhou J., et al. *J. Opt. Soc. Am. B*, **15**, 186 (1998).
171. Theberge F., Akozbek N., Liu W., et al. *Opt. Commun.*, **245**, 399 (2005).
172. Alexeev I., Ting A.C., Gordon D.F., et al. *Opt. Lett.*, **30** (12), 1503 (2005).
173. Lange H.R., Chiron A., Ripoche J.-F., et al. *Phys. Rev. Lett.*, **81**, 1611 (1998).
174. Painter J.C., Adams M., Brimhall N., et al. *Opt. Lett.*, **31**, 3471 (2006).
175. Theberge F., Akozbek N., Liu W., et al. *Phys. Rev. Lett.*, **97**, 023904 (2006).
176. Takao Fuji, Takuya Horio, Toshinori Suzuki. *Opt. Lett.*, **32**, 2481 (2007).
177. Tzortzakis S., Mechain G., Patalano G., et al. *Opt. Lett.*, **27** (21), 1944 (2002).
178. Akturk S., D'Amico C., Franco M., et al. *Phys. Rev. A*, **76**, 063819 (2007).
179. D'Amico C., Houard A., Franco M., et al. *Phys. Rev. Lett.*, **98**, 235002 (2007).
180. D'Amico C., Houard A., Franco M., et al. *Opt. Express*, **15**, 15274 (2007).
181. Sprangle P., Peåano J.R., Hafizi B., Kapetanakos C.A. *Phys. Rev. E*, **69** (6), 066415 (2004).
182. Ting-Ting Xi, Xin Lu, Jie Zhang. *Phys. Rev. Lett.*, **96**, 025003 (2006).
183. Hauri C.P., Kornelis W., Helbing F.W., et al. *Appl. Phys. B*, **79**, 673 (2004).
184. Hauri C.P., Guandalini A., Eckle P., et al. *Opt. Express*, **13** (19), 7541 (2005).
185. Xiaowei Chen, Xiaofang Li, Jun Liu, et al. *Opt. Lett.*, **32**, 2402 (2007).
186. Koprinkov I.G., Suda A.,Wang P., Midorikawa K. *Phys. Rev. Lett.*, **84** (17), 3847 (2000).
187. Li R., Chen X., Liu J., et al. *Proc. SPIE Int. Soc. Opt. Eng.*, **5708**, 102 (2005).
188. Kosareva O.G., Panov N.A., Uryupina D.S., et al. *Appl. Phys. B*, **8**, 2959 (2008).
189. Couairon A., Franco M., Mysyrowicz A., et al. *Opt. Lett.*, **30** (19), 2657 (2005).
190. Tzortzakis S., Berge L., Couairon A., et al. *Phys. Rev. Lett.*, **86**, 5470 (2001).
191. Kandidov V.P., Kosareva O.G., Shlenov S.A., et al. *Kvantovaya Elektron.*, **35**, 59 (2005) [*Quantum Electron.*, **35**, 59 (2005)**.**
192. Skupin S., Peschel U., Etrich C., et al. *Opt. Lett.*, **27** (20), 1812 (2002).
193. Hosseini S.A., Luo Q., Ferland B., et al. *Phys. Rev. A*, **70**, 033802 (2004).
194. Berge L., Skupin S., Lederer F., et al. *Phys. Rev. Lett.*, **92** (22), 225002 (2004).
195. Champeaux S., Berge L. *Opt. Lett.*, **31** (9), 1301 (2006).
196. Kosareva O.G., Panov N.A., Kandidov V.P. *Opt. Atmos. Okean.*, **18**, 223 (2005).
197. Luo Q., Hosseini S.A., Liu W., et al. *Appl. Phys. B*, **80**, 35 (2005).
198. Panov N.A., Kosareva O.G., Kandidov V.P., et al. *Proc. SPIE Int. Soc. Opt. Eng.*, **5708**, 91 (2005).
199. Zuo-Qiang Hao, Jie Zhang, Xin Lu, et al. *Opt. Express*, **14**, 773 (2006).
200. Mlejnek M., Kolesik M., Moloney J.V., Wright E.M. *Phys. Rev. Lett.*, **83**, 2938 (1999).
201. Chin S.L., Petit S., Borne F., Miyazaki K. *Jpn. J. Appl. Phys.*, **38**, L126 (1999).
202. Cook K., Kar A.K., Lamb R.A. *Appl. Phys. Lett.*, **83**, 3861 (2003).
203. Méjean G., Kasparian J., Yu J., et al. *Appl. Phys. B*, **82**, 341 (2006).
204. Ranka J.K., Schirmer R.W., Gaeta A.L. *Phys. Rev. Lett.,* **77**, 3783 (1996).
205. Mlejnek M., Wright E.M., Moloney J.V. *Opt. Express*, **4**, 223 (1999).
206. Kandidov V.P., Kiosareeva O.G., Mozhaev E.I., Tamarov M.P. *Opt. Atmos. Okean.*, **13**, 429 (2000).
207. Mechain G., Couairon A., Andre Y.-B., et al. *Appl. Phys. B*, **79**, 379 (2004).
208. Rodrigues M., Bourayou R., Méjean G., et al. *Phys. Rev. E*, **69**, 036607 (2004).
209. Jin Z., Zhang J., Xu M.H., et al. *Opt. Express*, **13**, 10424 (2005).
210. Fibich G., Sivan Y., Ehrlich Y., et al. *Opt. Express*, **14**, 4946 (2006).
211. Kandidov V.P., Golubtsov I.S., Kosareva O.G. *Kvantovaya Elektron.*, **34**, 348 (2004) [*Quantum Electron.*, **34**, 348 (2004)].
212. Mechain G., Couairon A., Franco M., et al. *Phys. Rev. Lett.*, **93**, 035003 (2004).
213. Grow T.D., Ishaaya A.A., Vuong L.T., et al. *Opt. Express*, **14**, 5468 (2006).
214. Dubietis A., Tamočauskas G., Fibich G., Ilan B. *Opt. Lett.*, **29** (10), 1126 (2004).
215. Fedorov V.Yu., Kandidov V.P., Kosareva O.G., et al. *Laser Phys.*, **16**, 1 (2006).
216. Mechain G., Couairon A., Franco M., et al. *Phys. Rev. Lett.*, **93**, 035003 (2004).
217. Grow T.D., Ishaaya A.A., Vuong L.T., et al. *Opt. Express*, **14**, 5468 (2006).
218. Kandidov V.P., Akozbek N., Skalora M., et al. *Kvantovaya Elektron.*, **34**, 879 (2004) [*Quantum Electron.*, **34**, 879 (2004)].
219. Kandidov V.P., Akozbek N., Scalora M., et al. *Appl. Phys. B*, **80**, 267 (2004).
220. Kandidov V.P., Dormidonov A.E., Kosareva O.G., et al. *Appl. Phys. B*, **87**, 29 (2007).
221. Kosareva O.G., Ngyen T., Panov N.A., et al. *Opt. Commun.*, **267**, 511 (2006).
222. Rohwetter P., Queißer M., Stelmaszczyk K., et al. *Phys. Rev. A*, **77**, 013812 (2008).
223. Fisher M., Siders C., Johnson E., et al. *Proc. SPIE Int. Soc. Opt. Eng.*, **6219**, 621907 (2006).
224. Fibich G., Eisenmann S., Ilan B., Zigler A. *Opt. Lett.*, **29** (15), 1772 (2004).
225. Liu J., Schroeder H., Chin S.L., et al. *Appl. Phys. Lett.*, **87**, 161105 (2005).
226. Panov N.A., Kosareva O.G., Kandidov V.P., et al. *Proc. SPIE Int. Soc. Opt. Eng.*, **5708**, 91 (2005).
227. Brabec T., Krausz F. *Phys. Rev. Lett.*, **78**, 3282 (1997).
228. Ranka J.K., Gaeta A.L. *Opt. Lett.*, **23**, 534 (1998).
229. Akozbek N., Scalora M., Bowden C.M., Chin S.L. *Opt. Commun.*, **191**, 353 (2001).
230. Sprangle P., Penano J.R., Hafizi B. *Phys. Rev. E*, **66**, 046418 (2002).
231. Kolesik M., Moloney J.V., Mlejnek M. *Phys. Rev. Lett.*, **89** (28), 283902 (2002).
232. Chzen Z., Mikhailova Yu.M., Platonenko V.T. *Pis'ma Zh. Eksp. Teor. Fiz.*, **85**, 482 (2007).
233. Kolesik M., Moloney J.V. *Phys. Rev. E*, **70**, 036604 (2004).
234. Kozlov S.A., Sazonov S.V. *Zh. Eksp. Teor. Fiz.*, **111**, 404 (1997).
235. Bespalov V.G., Kozlov S.A., Shpolyanskiy Y.A., Walmsley I.A. *Phys. Rev. A*, **66**, 013811 (2002).
236. Berkovsky A.N., Kozlov S.A., Shpolyanskiy Yu.A. *Phys. Rev. A*, **72**, 043821 (2005).
237. Bakhtin M.A., Kozlov S.A., Shpolyanskii Yu.A. *Opt. Spektrosk.*, **74**, 24 (2007).
238. Buyanovskaya E.M., Kozlov S.A. *Pis'ma Zh. Eksp. Teor. Fiz.*, **86**, 349 (2007).
239. Balashov A.D., Pergament A.Kh. *Preprint of M.V. Keldysh Institute of Applied Mathematics, RAS*, No. 40 (Moscow, 2004).
240. Bezborodov A.E., Shlenov S.A. *Izv. Ross. Akad. Nauk, Ser. Fiz.*, **70**, 1246 (2006).
241. Vorob'ev V.V. *Izv. Vyssh. Uchebn. Zaved., Ser. Radiofiz.*, **23**, 905 (1970).
242. Akozbek N., Bowden C.M., Talebpour A., Chin S.L. *Phys. Rev. E*, **61**, 4540 (2000).

243. Bulygin A.D., Geints Yu.E., Zemlyanov A.A. *Opt. Atmos. Okean.*, **20**, 973 (2007).
244. Raizer Yu.P. *Fizika gazovogo razryada* (Physics of a Gas Discharge) (Moscow: Nauka, 1992).
245. Talebpour A., Yang J., Chin S.L. *Opt. Commun.*, **163**, 29 (1999).
246. Perelomov A.M., Popov V.S., Terent'ev M.V. *Zh. Eksp. Teor. Fiz.*, **50**, 1393 (1966); Popov V.S. *Usp. Fiz. Nauk*, **174**, 921 (2004)
247. Amosov M.V., Delone N.B., Krainov V.P. *Zh. Eksp. Teor. Fiz.*, 91, 2008 (1986).
248. Perry M.D., Landen O.L., Szoke A., Campbel F.M. *Phys. Rev. A*, **37**, 747 (1988).
249. Mao S.S., Quere F., Guizard S., et al. *Appl. Phys. A*, **79**, 1695 (2004).
250. Kenichi Ishikawa, Hiroshi Kumagai, Katsumi Midorikawa. *Phys. Rev. E*, **66**, 056608 (2002).
251. Couairon A., Sudrie L., Franco M., et al. *Phys. Rev. B*, **71**, 125435 (2005).
252. Rethfeld B. *Phys. Rev. Lett.*, **92**, 187401 (2004); *Phys. Rev. B*, **73**, 035101 (2006).
253. Chin S.L., Talebpour A., Yang J., et al. *Appl. Phys. B*, **74**, 67 (2002).
254. Kandidov V.P., Kosareva O.G., Tamarov M.P., et al. *Kvantovaya Elektron.*, **27**, 73 (1999) [*Quantum Electron.*, **29**, 355 (1999)].
255. Shlenov S.A., Kandidov V.P., Kosareva O.G. *Techn. Dig. IQEC/ LAT-2002* (Moscow, Russia, 2002) p. 53; *Techn. Progr. XI Conf. on Laser Optics (LO'2003)* (St.Petersburg, Russia, 2003) p. 43.
256. Ackermann R., Méjean G., Kasparian J., et al. *Opt. Lett.*, **31** (1), 86 (2006).
257. Shlenov S.A., Kandidov V.P. *Opt. Atmos. Okean.*, **17**, 637 (2004).
258. Salamé R., Lascoux N., Salmon E., et al. *Appl. Phys. Lett.*, **91**, 171106 (2007).
259. Shlenov S.A., Kandidov V.P. *Opt. Atmos. Okean.*, **17**, 630 (2004).
260. Penano J.R., Sprangle P., Hafizi B., et al. *Phys. Plasmas*, **11** (5), 2865 (2004).
261. Kandidov V.P., Shlenov S.A., Kosareva O.G., et al. *Proc. SPIE Int. Soc. Opt. Eng.*, **6733**, 67332M (2007).
262. Shlenov S.A., Kandidov V.P. *Izv. Ross. Akad. Nauk, Ser. Fiz.*, **69**, 1121 (2005).
263. Mechain G., Méjean G., Ackermann R., et al. *Appl. Phys. B*, **80** (7), 785 (2005).
264. Kandidov V.P., Militsin V.O. *Appl. Phys. B*, **83**, 171 (2006); Kandidov V.P., Militsin V.O. *Opt. Atmos. Okean.*, **19**, 765 (2006).
265. Militsin V.O., Kuz'minskii L.S., Kandidov V.P. *Opt. Atmos. Okean.*, **18**, 880 (2005).
266. Militsyn V.O., Kachan E.P., Kandidov V.P. *Kvantovaya Elektron.*, **36**, 1032 (2006) [*Quantum Electron.*, **36**, 1032 (2006)].
267. Bochkarev N.N., Zemlyanov An.A., Zemlyanov A.A., et al. *Opt. Atmos. Okean.*, **17**, 971 (2004).
268. Bagaev S.N., Geints Yu.E., Zemlyanov A.A., et al. *Opt. Atmos. Okean.*, **20**, 413 (2007).
269. Méjean G., Kasparian J., Yu J., et al. *Phys. Rev. E*, **72** (2), 026611 (2005).
270. Zemlyanov A.A., Geints Yu.E. *Opt. Commun.*, **259** (2), 799 (2006).
271. Kolesik M., Moloney J.V. *Opt. Lett.*, **29** (6), 590 (2004).
272. Liu W., Théberge F., Daigle J.-F., et al. *Appl. Phys. B*, **85**, 55 (2006).
273. Nuter R., Skupin S., Berge L. *Opt. Lett.*, **30** (8), 917 (2005).
274. Nuter R., Berge L. *J. Opt. Soc. Am. B*, **23** (5), 874 (2006).
275. Couairon A., Franco M., Mechain G., et al. *Opt. Commun.*, **259**, 265 (2006).
276. Shlenov S.A., Fedorov V.Yu., Kandidov V.P. *Opt. Atmos. Okean.*, **20**, 378 (2007).
277. Mechain G., Olivier T., Franco M. *Opt. Commun.*, **261**, 322 (2006).
278. Bernhardt J., Liu W., Chin S.L., Sauerbrey R. *Appl. Phys. B*, **91**, 45 (2008).
279. Zemlyanov A.A., Geints Yu.E. *Opt. Atmos. Okean.*, **18**, 868 (2005).
280. Kasparian J., Bourayou R., Boutou V., et al. *Proc. SPIE Int. Soc. Opt. Eng.*, **5226** (1), 238 (2003).
281. Gordienko V.M., Kholodnykh A.I., Pryalkin V.I. *Kvantovaya Elektron.*, **30**, 839 (2000) [*Quantum Electron.*, **30**, 839 (2000)].
282. Bourayou R., Méjean G., Kasparian J., et al. *J. Opt. Soc. Am. B*, **22** (2), 369 (2005).
283. Rairoux P., Schillinger H., Niedermeier S., et al. *Appl. Phys. B*, **71**, 573 (2000).
284. Yu J., Mondelain D., Ange G., et al. *Opt. Lett.*, **26** (8), 533 (2001).
285. Rohwetter Ph., Yu J., Méjean G., Stelmaszczyk K. *J. Anal. Atom Spectrom.*, **19**, 437 (2004).
286. Hashida M., Semerok A.F., Gobert O., et al. *Appl. Surf. Sci.*, **197-198**, 862 (2002).
287. Liu W., Xu H.L., Méjean G., et al. *Spectrochim. Acta. Pt B*, **62**, 76 (2007).
288. Xu H.L., Bernhardt J., Mathieu P., et al. *J. Appl. Phys.*, **101**, 033124 (2007).
289. Tzortzakis S., Anglos D., Gray D. *Opt. Lett.*, **31** (8), 1139 (2006).
290. Xu H.L., Liu W., Chin S.L. *Opt. Lett.*, **31** (10), 1540 (2006).
291. Xu H.L., Méjean G., Liu W., et al. *Appl. Phys. B*, **87**, 151 (2007).
292. Daigle J.-F., Méjean G., Liu W., et al. *Appl. Phys. B*, **87** (4), 749 (2007).
293. La Fontaine B., Comtois D., Chien C.-Y., et al. *J. Appl. Phys.*, **88**, 610 (2000).
294. Rodrigues M., Sauerbrey R., Wille H., et al. *Opt. Lett.*, **27** (9), 772 (2002).
295. Ackermann R., Mechain G., Méjean G., et al. *Appl. Phys. B*, **82**, 561 (2006).
296. Mechain G., Ackermann R., Kasparian J., et al. *Appl. Phys. Lett.*, **88**, 021101 (2006).
297. Houard A., D'Amico C., Liu Y., et al. *Appl. Phys. Lett.*, **90**, 171501 (2007).
298. Fujii T., Miki M., Goto N., et al. *Phys. Plasmas*, **15**, 013107 (2008).
299. Ackermann R., Stelmaszczyk K., Rohwetter P., et al. *Appl. Phys. Lett.*, **85**, 5781 (2004).
300. Kasparian J., Ackermann R., Andre Y.-B., et al. *Opt. Express*, **16**, 5757 (2008).
301. Valuev V.V., Kandidov V.P., Cherepenin V.A. *Integral*, No. 6, 6 (2006).
302. Dormidonov A.E., Valuev V.V., Dmitriev V.L., et al. *Proc. SPIE Int. Soc. Opt. Eng.*, **6733**, 67332S (2007).
303. Châteauneuf M., Payeur S., Dubois J., Kiefer J.-C. *Appl. Phys. Lett.*, **92**, 091104 (2008).
304. Musin R.R., Shneider M.N., Zheltikov A.M., Miles R.B. *Appl. Opt.*, **46**, 5593 (2007).
305. Homoelle D., Wielandy S., Gaeta A.L., et al. *Opt. Lett.*, **24**, 1311 (1999).
306. Chan J.W., Huser T., Risbud S., Krol D.M. *Opt. Lett.*, **26**, 1726 (2001).
307. Sung-Hak Cho, Hiroshi Kumagai, Katsumi Midorikawa. *Opt. Commun.*, **207**, 243 (2002).
308. Quan Sun, Hongbing Jiang, Yi Liu, et al. *Opt. Lett.*, **30**, 320 (2005).
309. Zoubir A., Richardson M., Canioni L., et al. *J. Opt. Soc. Am. B*, **22**, 2138 (2005).
310. Sudrie L., Franco M., Prade B., Myzyrowicz A. *Opt. Commun.*, **171**, 279 (1999); **191**, 333 (2001).
311. Poumellec B., Sudrie L., Franco M., et al. *Opt. Express*, **11**, 1070 (2003).
312. Hengchang Guo, Hongbing Jiang, Ying Fang, et al. *J. Opt. A: Pure Appl. Opt.*, **6**, 787 (2004).
313. Gattass R.R., Cerami R.L., Mazur E. *Opt. Express*, **14**, 5279 (2006).
314. Nguen N.T., Saliminia A., Chin S.L., Vallee R. *Appl. Phys. B*, **85**, 145 (2006).
315. Takayuki Tamaki, Wataru Watanabe, Hiroyuki Nagai, et al. *Opt. Express*, **14**, 6971 (2006).

316. Yamada K., Watanabe W., Nishii J., Itoh K. *J. Appl. Phys.*, **93**, 1889 (2003).
317. Onda S., Watanabe W., Yamada K., Itoh K. *J. Opt. Soc. Am. B*, **22**, 2437 (2005).
318. Tokyda Y., Saito M., Takahashi M., et al. *J. Non-Cryst. Solids*, **326-327**, 472 (2003).
319. Streltsov A.M., Borrelli N.F. *J. Opt. Soc. Am. B*, **19**, 2496 (2002).
320. Watanabe W., Asano T., Yamada K., Itoh K. *Opt. Lett.*, **28**, 2491 (2003).
321. Minoshima K., Kowalevicz A.M., Hartl I., et al. *Opt. Lett.*, **26**, 1516 (2001).
322. Chen H., Chen X., Xia Y., et al. *Opt. Express*, **15**, 5445 (2007).
323. Szameitt A., Blomer D., Burghoff J., et al. *Appl. Phys. B*, **82**, 507 (2006).
324. Yamada K., Watanabe W., Li Y., et al. *Opt. Lett.*, **29**, 1846 (2004).
325. Cheng Y., Sugioka K., Midorikawa K., et al. *Opt. Lett.*, **28**, 1144 (2003).